

---

Mechanical Engineering Theses

Mechanical Engineering

---

Spring 5-14-2020

## Effects of Hard-to-Soft Segment Ratios on the Synthesis and Physico-mechanical Properties of Polyurethane Films

Aaron C. Wilson  
*University of Texas at Tyler*

Follow this and additional works at: [https://scholarworks.uttyler.edu/me\\_grad](https://scholarworks.uttyler.edu/me_grad)

 Part of the [Biomaterials Commons](#), [Biomechanical Engineering Commons](#), and the [Polymer and Organic Materials Commons](#)

---

### Recommended Citation

Wilson, Aaron C., "Effects of Hard-to-Soft Segment Ratios on the Synthesis and Physico-mechanical Properties of Polyurethane Films" (2020). *Mechanical Engineering Theses*. Paper 13.  
<http://hdl.handle.net/10950/2590>

This Thesis is brought to you for free and open access by the Mechanical Engineering at Scholar Works at UT Tyler. It has been accepted for inclusion in Mechanical Engineering Theses by an authorized administrator of Scholar Works at UT Tyler. For more information, please contact [tgullings@uttyler.edu](mailto:tgullings@uttyler.edu).

EFFECTS OF HARD-TO-SOFT SEGMENT RATIOS ON THE  
SYNTHESIS AND PHYSICO-MECHANICAL PROPERTIES OF  
POLYURETHANES

by

AARON WILSON

A thesis submitted in partial fulfillment  
of the requirements for the degree of  
Master of Science  
Department of Mechanical Engineering

Shih-Feng Chou, Ph.D., Committee Chair  
College of Engineering

The University of Texas at Tyler  
May 2020

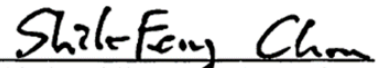
The University of Texas at Tyler  
Tyler, Texas

This is to certify that the Master's Thesis of

AARON WILSON

has been approved for the thesis requirement on  
April 10, 2020  
for the Master of Science degree

Approvals:



Thesis Chair: Shih-Feng Chou, Ph.D.



Member: Fredericka Brown, Ph.D.



Member: Nelson Fumo, Ph.D.



Chair, Department of Mechanical Engineering

 FOR JK

Dean, College of Engineering

The style and format of this thesis are in accordance with **Materials Science and Engineering C: Materials for Biological Applications**. The following referred journal papers and conference proceedings were products of the M.S. degree:

**Referred Journal Articles:**

- [1] **A.C. Wilson**, P. Neuenschwander, S.F. Chou, Engineering approaches to prevent blood clotting from medical implants, Archives in<sup>[1]</sup><sub>SEP</sub> Biomedical Engineering & Biotechnology, 1 (2019) 5. doi:10.33552/ABEB.2018.01.000510.
- [2] **A.C. Wilson**, S.F. Chou, R. Lozano, J.Y. Chen, P. Neuenschwander, Thermal and physico-mechanical characterizations of thromboresistant polyurethane films, Bioengineering, 6 (2019) 69. doi:10.3390/bioengineering6030069.

**Conference Proceedings:**

- [1] **A. Wilson**, A. Craig, P. Neuenschwander, S.F. Chou, (2019), The use of polymeric coatings for anticoagulation on implantable medical devices, In Proceedings of the 2019 ASEE Gulf-Southwest Section Annual Meeting, Tyler TX. *Best Paper Award*.

## Acknowledgements

I would like to first express my sincere gratitude to Dr. Shih-Feng Chou for giving me the opportunity to perform this research under his guidance and for his continuous support, patience, and encouragement. It has truly been a privilege to work with him on this research. I would like to give special thanks to my committee members, Dr. Fredericka Brown and Dr. Nelson Fumo, for their valuable advice and support, as well as Dr. Pierre Neuenschwander (Department of Cellular & Molecular Biology, UT Health Science Center at Tyler) for his guidance and support.

I would like to thank Madeline Small and Alex Craig for their assistance and support, as well as Addison Faglie and the other members of the Biomaterials Lab for their support and encouragement. Lastly, I would like to thank my family for their unending support and encouragement.

## Table of Contents

List of Tables .....	iv
List of Figures .....	v
Abstract .....	ix
Chapter 1: Introduction .....	1
Chapter 2: Significance .....	4
Chapter 3: Literature Review .....	6
3.1 Clotting Cascade .....	6
3.2 Anticoagulation Coatings .....	8
3.2.1 Biocompatibility .....	8
3.2.2 Coatings that Improved Existing Devices.....	8
3.2.3 Polymeric Coatings .....	9
3.2.4 Non Polymeric Coatings .....	11
3.2.5 Surface Modifications to Coatings.....	13
3.2.6 Polyurethanes .....	15
Chapter 4: Materials and Methods .....	16
4.1 Materials .....	16
4.2 Preparations of Polyurethane Commercial Films .....	16
4.3 Synthesis of Polyurethane Samples .....	16
4.4 Fourier-Transform Infrared Spectroscopy (FTIR).....	18
4.5 Differential Scanning Calorimetry (DSC) .....	18
4.6 Thermal Gravimetric Analysis (TGA).....	19

4.7 X-Ray Diffraction (XRD).....	19
4.8 Water Contact Angle and Water Absorption.....	19
4.9 Mechanical Testing.....	20
4.10 Clotting Assays.....	20
Chapter 5: Results and Discussion.....	22
5.1 Commercial PU Films .....	22
5.1.1 Appearance.....	22
5.1.2 FTIR.....	23
5.1.3 DSC.....	25
5.1.4 TGA .....	27
5.1.5 XRD .....	29
5.1.6 Water Content Angle and Water Absorption.....	30
5.1.7 Mechanical Properties.....	32
5.1.8 Clotting Assays .....	35
5.2 Films Synthesized In Lab .....	39
5.2.1 Synthesis .....	39
5.2.2 Yield Mass .....	41
5.2.3 Physical Appearance and Characteristics .....	43
5.2.4 FTIR Analysis.....	45
5.2.5 Water Content Angle Studies.....	46
5.2.6 Water Absorption and Degradation Studies .....	47
5.2.7 Mechanical Properties.....	49

5.2.8 Comparison to Commercial Films .....	53
Chapter 6: Conclusions and Future Work.....	55
References.....	58



## List of Tables

<b>Table 1.</b> Summary of current anticoagulant coatings.....	13
<b>Table 2.</b> dTG temperatures and their corresponding percentage mass losses of the commercial PU films. ....	29
<b>Table 3.</b> Comparison of mechanical properties of the commercial films to the lab films. .....	54

## List of Figures

<b>Figure 1.</b> Schematic illustration of the blood clotting cascade. ....	7
<b>Figure 2.</b> Laboratory setup for polyurethane synthesis, thermometer is included in beaker due to an inaccurate hot plate temperature.....	17
<b>Figure 3.</b> Visual representation of the precipitation process of the polyurethane samples. ....	18
<b>Figure 4.</b> Physical appearance of the four commercial PU films: from left to right in the top wells, 200ET, 100ES, 60ES, and 60ET. The second row of 4 wells contains no PU films for comparison of the transparency of the PU films.....	22
<b>Figure 5.</b> FTIR spectra of the various commercial PU films for: (a) wavenumbers from 650 $\text{cm}^{-1}$ to 4000 $\text{cm}^{-1}$ showing the characteristic peaks of N–H stretching vibration at around 3300 $\text{cm}^{-1}$ and C=O stretching vibration from amide I band at around 1700 $\text{cm}^{-1}$ ; (b) wavenumbers from 1000 $\text{cm}^{-1}$ to 1600 $\text{cm}^{-1}$ showing the characteristic peaks of N–H bending vibration from amide II band at around 1531 $\text{cm}^{-1}$ and C–N stretching vibration from amide III band at around 1314 $\text{cm}^{-1}$ that form the urethane linkage (–NHCO–).....	25
<b>Figure 6.</b> DSC thermograms of the various PU films from 25°C to 200°C, where a thermal endotherm at approximately 50°C for the 200ET groups corresponds to melting of the soft segments. ....	27
<b>Figure 7.</b> Thermal stability evaluations of the various PU films, showing (a) representative TGA curves on percentage mass loss with onset temperatures ranged between 337 °C to 355 °C; (b) representative dTG curves where 60ES and 100ES	

groups exhibited single peak decomposition temperature and 60ES and 200ES	
groups displayed a two-step decomposition process. ....	28
<b>Figure 8.</b> XRD patterns of the various PU films, showing a broad peak at $2\theta = 20^\circ$	
related to semicrystalline structure of the hard/soft segments in PUs. The small	
peaks at the shoulders of the 100ES and 60ET groups were attributed to the partial	
crystallization of the soft segments. ....	30
<b>Figure 9.</b> (a) Water contact angle study on the various commercial PU films comparing	
to a glass control. (b) Water absorption and/or degradation study on various	
commercial PU films over 14 days. Figure inset shows short-term study up to 2 h.	32
<b>Figure 10.</b> Mechanical properties of the various PU films, showing (a) a representative	
engineering stress-strain curve from 200ET groups; (b) average elastic moduli; (c)	
average elongation to failure; (d) average tensile strength. ....	35
<b>Figure 11.</b> In vitro clotting assays on the various PU films in comparison with the glass	
control, showing (a) clotting assay (1) where human blood plasma were placed on	
the surface of the activating substances; (b) effects of $\text{CaCl}_2$ concentrations on the	
clot times using clotting assay (1); (c) clotting assay (2) where human blood plasma	
and the activating substances were placed in an enclosure. ....	39
<b>Figure 12.</b> PU samples synthesized and precipitated in the lab at various PEG:TDI ratios,	
including 1:20, 1:40, 1:80, and 1:160, using step polymerization. ....	40
<b>Figure 13.</b> Standard heating times for the step polymerization of the PU samples from	
mixtures of PEG:TDI at different ratios. ....	42

<b>Figure 14.</b> The relationship of yield mass obtained from the precipitated PU samples and the PEG:TDI ratios in the mixture for step polymerization.....	43
<b>Figure 15.</b> Physical appearance of the synthesized PU films at different ratios of PEG:TDI without the chain extender BDO: (a) 1:20, (b) 1:40, (c) 1:80, and (d) 1:160 (PEG:TDI) ratio. ....	44
<b>Figure 16.</b> FTIR spectra of the synthesized PU samples for wavenumbers from 700 cm <sup>-1</sup> to 4000 cm <sup>-1</sup> showing the characteristic peaks of N–H stretching vibration at around 3300 cm <sup>-1</sup> and C=O stretching vibration from amide I band at around 1700 cm <sup>-1</sup> , as well as wavenumbers from 1000 cm <sup>-1</sup> to 1600 cm <sup>-1</sup> showing the characteristic peaks of N–H bending vibration from amide II band at around 1531 cm <sup>-1</sup> and C–N stretching vibration from amide III band at around 1314 cm <sup>-1</sup> that form the urethane linkage (–NHCO–).....	45
<b>Figure 17.</b> Water contact angle study on the various lab-synthesized PU films.....	47
<b>Figure 18.</b> (a) Short-term water absorption and/or degradation study on the lab-synthesized PU films without BDO over 2 hours. (b) Long-term water absorption and/or degradation study on the lab-synthesized PU films without BDO over 14 days. ....	48
<b>Figure 19.</b> (a) Short-term water absorption and/or degradation study on the lab-synthesized PU films with BDO over 2 hours. (b) Long-term water absorption and/or degradation study on the lab-synthesized PU films with BDO over 14 days.....	49
<b>Figure 20.</b> Representative engineering stress-strain curves of the various lab-synthesized PU film ratios without BDO: (a) All ratios, (b) 1:40, 1:80, and 1:160 films.....	50

<b>Figure 21.</b> Representative engineering stress-strain curves of the various lab-synthesized PU film ratios with BDO: (a) All ratios, (b) 1:40, 1:80, and 1:160 films. ....	51
<b>Figure 22.</b> (a) Average elastic moduli of the various lab-synthesized PU film ratios, with and without BDO. (b) Average tensile strength of the various lab-synthesized PU film ratios, with and without BDO. (c) Average elongation to failure of the various lab-synthesized PU film ratios, with and without BDO. ....	53

## Abstract

### EFFECTS OF HARD-TO-TOFT SEGMENT RATIOS ON THE SYNTHESIS AND PHYSICO-MECHANICAL PROPERTIES OF POLYURETHANES

Aaron Wilson

Thesis Chair: Shih-Feng Chou, Ph.D.

The University of Texas at Tyler  
May 2020

Blood-contacting cardiovascular stents often induce a secondary clotting event due to unrestricted enzymatic activities. The use of hemocompatible polyurethane coatings on these implantable devices is one of the most promising methods to reduce device rejection. In this study, four commercial polyurethane films of various thicknesses and compositions were evaluated for their anticoagulation properties. Results suggested that these films exhibited excellent thermal and physico-mechanical properties while capable of increasing contact time with blood plasma by over a thousand-fold as compared to a control surface. Due to the unknown structure and composition of these commercial films, polyurethane samples were synthesized from toluene diisocyanate as the hard segment and polyethylene glycol as the soft segment under various hard-to-soft segment ratios. The synthesized samples were cast into films for testing of their physico-mechanical properties. The effects of the hard-to-soft segment ratios on these properties and the synthesis process were evaluated in order to optimize them for use in anticoagulation coatings.

## Chapter 1: Introduction

With the many diseases and disabilities faced in the medical field today, one of the most common and serious occurrences is blood clotting. Venous thromboembolisms (VTE), which are clots that form in blood veins, affects 300,000-600,000 people per year in the US and kills roughly 90,000 of those affected [1]. Operations for this can be quite costly as well, as the average operation cost to remove a deep vein clot is \$10,000. In fact, clot removal operations can range in cost from \$1,000-\$100,000 per operation, depending on the severity and location of the clot, and there is typically a 10-50% copay with insurance [2]. One contributing factor is heart disease, which affects 28.2 million adults in the US or 11.5% of the adult population and is the #1 cause of death in the US, claiming 650,000 lives per year [3]. Other related factors include implantable devices such as cardiovascular stents, 1.8 million of which are implanted in the US per year at a cost of \$35,000-\$40,000 per operation and 10-20% with insurance [4,5].

Depending on the severity of the clot, a number of treatments are available. If it is not too serious, a doctor may prescribe medication, such as heparin, or advise the use of a compression wrap [6]. More serious clots or those in vital areas will require an operation. For those vital areas, one of the most popular options is the implantation of a vascular stent, which is inserted into the blocked blood vessel to help blood flow freely. Vascular stents act as structural support during the regrowth of the endothelial cells that coat the walls of vessels and are capable of other functions, such as drug delivery. However, inserting foreign objects into the body can have very serious consequences, namely the activation of the coagulation cascade, which is the process of clot formation that is

normally activated to make repairs to damaged areas. It can be life-threatening for a patient as it is also capable of closing off blood flow to major arteries and vessels.

One of the most attractive and innovative methods for solving this issue is the use of a hemocompatible coating along the surface of these devices to minimize the possibility of the clotting process to be activated [7]. Several types of coatings have been examined for this use and one of the most promising is polyurethane coatings [8].

Polyurethanes are created by mixing a soft segment, consisting of a polyol, and a hard segment, made from a combination of a diisocyanate and a low molecular weight diol or diamine, at specific stoichiometric ratios [9]. The functional groups of each segment, OH groups for the soft segment and NCO groups for the hard segment, combine to form NCOOH urethane bonds, the formation of which can be seen using FTIR analysis [10,11]. The ratio of the hard-to-soft segments has a large impact on the properties of the polyurethane. Therefore, the purpose of this work is to study the effects of the ratio of the components used to synthesize the PU samples on the synthesis process and the physico-mechanical properties of the samples. This is done to help optimize the properties of the PU for use as anticoagulation coatings on implantable medical devices.

In this work, currently available coatings are compared, and polyurethane (PU) coatings show promising potential. Therefore, four commercial PU films, two polyester urethane films and two polyether urethane films of various thicknesses and shore hardness, were purchased. The physical appearance of the films was determined, then the chemical structure of the PU films was evaluated using Fourier-transform infrared (FTIR) spectroscopy. Next, the thermal properties of these films were determined through the use



of differential scanning calorimetry (DSC) and thermal gravimetric analysis (TGA) as well as their crystallinity by using X-ray diffraction (XRD) technique. The physico-mechanical properties of the PU films were then determined by water contact angle and water absorption/degradation studies along with tensile testing. Lastly, in vitro clotting assays were performed using human blood plasma on the various PU films to determine their anticoagulant properties. Based on the results of this testing, an ester-based polyurethane that could be synthesized with a simple laboratory setup was developed and several samples of various composition ratios were successfully synthesized. The physico-mechanical properties of these films were then evaluated to determine the effects of the ratios and their viability as anticoagulation coatings on implantable medical devices.

## Chapter 2: Significance

The significance of this thesis work is the early steps towards producing an anticoagulation coating that will significantly reduce the chance of implanted biomedical devices to be rejected in the body over a long period of time. While there are commercially available anticoagulation films currently available, the films created for this work are unique. Currently used films are able to delay the clot formation process for years, but many of them are designed to break down and release drugs that aid in preventing clotting. Once these films completely break down, the risk of clotting will again become significant. While this may be fine for patients who unfortunately only live for a few years after receiving an implanted device, others may live for twenty or more years after receiving the implant. In order to improve their quality of life and potentially extend their lifespan, it is imperative that a longer-lasting solution be found.

The uniqueness of this work is that the films synthesized were designed with longevity in mind. Polyurethanes were used as the base of these films because they are both naturally versatile and easily modified. There are plenty of options available to use for the soft and hard segments with several studies done on the biocompatibility of many of the materials, as well as on surface modifications that can be made to polyurethane films in order to significantly change certain properties. None of the currently available coatings have been found to last more than a few years after implantation, therefore, designing a new coating and modifying it appropriately to prevent clotting over a much longer period of time without the use of drugs would be a significant improvement over

available commercial options for anticoagulation coatings on implantable biomedical devices.

## Chapter 3: Literature Review

### 3.1 Clotting Cascade

In order to establish whether a polymeric coating can be an effective tool for anticoagulation, it is necessary to first understand how the body will react when introduced to these materials [12]. There are two paths through which the clotting process commences, the tissue factor pathway and the contact pathway. The tissue factor pathway is the natural process by which the body heals itself of injuries, like cuts to the skin. The contact pathway is activated when foreign objects, such as implantable medical devices, come into contact with the blood. This contact triggers a change in the structure (activation) of a plasma protein called factor XII, which becomes active factor XII (XIIa). The presence of XIIa then activates the enzyme plasma prekallikrein (PK) into kallikrein, which further activates XII, leading to a mass production of XIIa. Factor XIIa then activates the enzyme factor XI into XIa, which breaks down the protein factor IX into IXa through proteolysis, which then activates factor X into Xa. Once factor Xa is finally triggered by the flood of other enzymes and proteins in the blood that are activated during the coagulation cascade, the process concludes with the generation of the enzyme thrombin, which polymerizes the protein fibrinogen into fibrin and the activation of platelets, both of which form blood clots [13–15].

The reason that this cascade occurs is that blood is usually only in contact with the walls of the vessels that carry them through the circulatory system. These vessels are coated with endothelial cells, which perform a range of useful functions when healthy, including the prevention of clotting. The clotting cascade, which is visually represented

in Figure 1, begins when these cells are damaged, as the damaged surface becomes thrombotic [16].

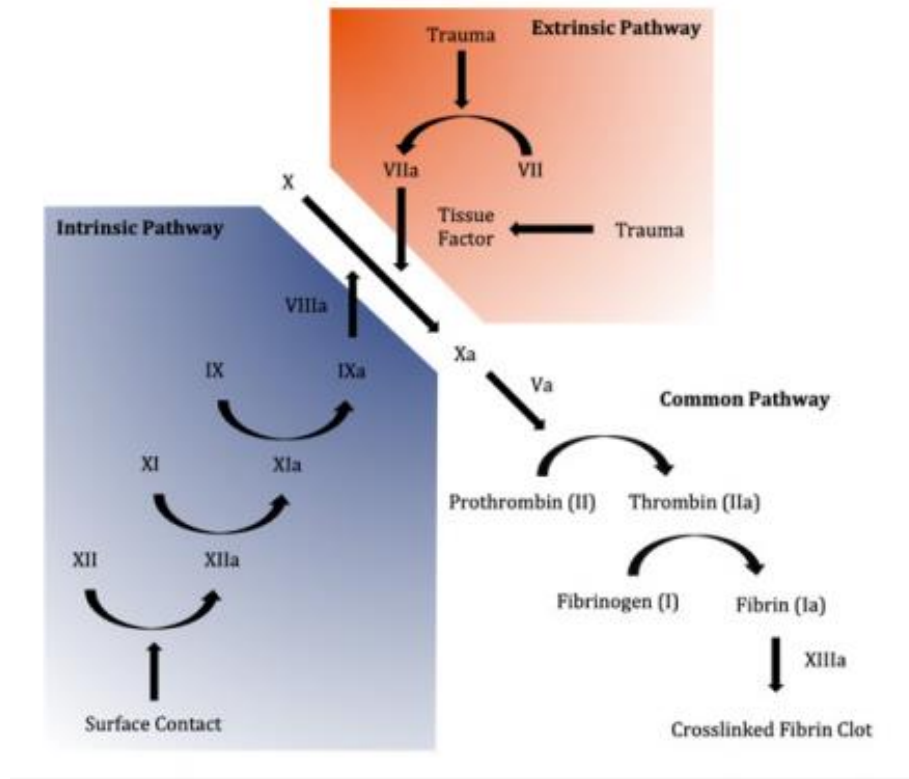


**Figure 1.** Schematic illustration of the blood clotting cascade.

Seeing as implantable devices are not coated with a layer of endothelial cells, the body considers them to be a damaged vessel surface and will begin the clotting process to attempt to repair it. However, unlike the normal process of forming clots inside holes along the surface of a vessel, clots will begin to form on the outside surface of the biomaterial. This not only raises the risk that the implanted device will fail but could potentially be very harmful or even fatal to the recipient, as this could cause the blood

flow in vessels and arteries to be entirely cut off. One possible solution that researchers are looking at to prevent this is the use of anticoagulant coatings for implantable devices.

### **3.2 Anticoagulation Coatings**

#### **3.2.1 Biocompatibility**

When determining the suitability of biomaterials for anticoagulation, biocompatibility is one of the most important factors to consider. The key aspects that must be examined before the use of a biomaterial is considered are: is the body going to immediately attack or reject the material, can the material cause the formation of tumors in the neighboring tissue, and is the material prothrombotic [17]. As the last factor is the basis of finding suitable coatings for anticoagulation, the other factors are the more crucial problems to consider.

#### **3.2.2 Coatings that Improved Existing Devices**

Of the many implantable devices currently in use, one that could seriously benefit from the addition of improved anticoagulation coatings is the cardiovascular stent. Stents are routinely used to hold clogged arteries open to allow for better blood flow, with the most frequently used types of stents being bare metal stents and drug-eluting stents. Bare metal stents are meshes composed of different types of metals and alloys that can be expanded inside a vessel, and drug-eluting stents, which are made of the same mesh material, also include a biodegradable polymeric coating that breaks down and releases anticoagulation and antiproliferative agents into the blood over time [18].

Thanks to the addition of the biodegradable coating, drug-eluting stents are considered to be the safer option, as they have been proven to have a lower risk of causing clot formation. However, the coatings used on these stents only last a few months before they dissolve completely. This means that clots can still form over time inside these stents, even in combination with double antiplatelet therapy, which helps to further prevent clot formation [19,20]. To reduce the possibility that clotting occurs, the coatings for these stents need to either dissolve at a much slower rate or have the ability to administer the drug without dissolving the polymer entirely.

### **3.2.3 Polymeric Coatings**

Heparin, an excellent anticoagulant drug that is also effective for controlling immune defense and cell growth has been one of the most popular methods for avoiding thrombosis for decades. Grafting or ionically attaching heparin to the surface of a polymer coating can significantly increase its effectiveness at preventing clots, and coatings with heparin attached have been shown to reduce clot formation by over 70% [18]. However, as effective as heparin use can be, it has a few disadvantages. In addition to being a great anticoagulant, it is also a blood thinner, which raises the chance for severe bleeding to occur. Also, heparin-induced thrombocytopenia (HIT), a possible side effect due to repeated use of heparin, is a prothrombotic disorder that can increase the risk that clots form around the coated device [21].

This has led to the development of synthetic polymer coatings meant to mimic the anticoagulant properties of heparin without the side effects, which could be especially beneficial for patients that rely on the drug, such as those going through dialysis

treatments. This was done by finding the chemical properties that are believed to be the basis for heparin's clot prevention abilities, the presence of abundant sulfate or carboxyl groups, and creating polymers with similar chemical structures. Wang et al. coated a polylactide (PLA) membrane with one of these heparin-mimicking polymers synthesized with methylacrylic acid (MAA) and ethylene glycol diacrylate (EGDA) and noted that the coated membranes were capable of mimicking the effects of heparin, as the membranes exhibited extended clotting times and reduced platelet adhesion [21].

Polyurethanes are another type of polymeric coating that is becoming more popular for potential anticoagulant coating applications, thanks in part to the ease of modification to these polymers. Chi et al. [22] purchased a commercial polyurethane film and modified it with 2-methacryloyloxyethyl phosphorylcholine (MPC). Results obtained from testing displayed enhanced resistance to platelet adhesion, increased hydrophilicity, and only a very small amount of plasma calcium was able to be retrieved during clotting trials, even after multiple tests. All of these properties show very promising potential for anticoagulation, however, the reasons for the film's excellent properties could not be explained. If these results prove to be reliable, then the anticoagulation properties of this modified polyurethane film are phenomenal [22].

Other trials using modified polyurethane films have not proved as successful. Graphene and tricalcium phosphate (TCP) were added during the production of a polyurethane composed of polyethylene glycol (PEG), 4,4'-diisocyanate diphenylmethane (MDI), and 1,4-butanediol (BDO) as a chain extender that was going to be used to coat titanium plates. The focus of the testing performed was aimed more



towards the film's antibacterial properties and found that using 4wt% graphene in the polymer made the coating cytotoxic, making it worthless for the intended purpose. Lower amounts of graphene, such as 0.25 wt%, did not have the same effect, but for this combination to be considered for use as a biomaterial, it will need to be tested further [23].

Amoako et al. [24] devised a creative idea for an anticoagulant coating and attempted to “create an artificial endothelium by coupling anti-fouling zwitterionic functional groups, similar to those expressed by endothelial cells, with anti-platelet nitrous oxide, which is released by endothelial cells.” Their hypothesis was that the combination of these methods would result in a highly effective coating, and the reduction of platelet adsorption by over 90% obtained during testing proved their hypothesis [24].

Other variations and combinations of these methods have been attempted to help improve current anticoagulation coatings. Non-eluting heparin coatings, graphene oxide on titanium, and graphene with heparin attached have all been recently explored as potential options [25,26]. These options, however, do not resolve the issues of the individual methods, as the possible cytotoxicity of graphene and HIT caused by frequent heparin use are still possible consequences of using these materials [21,23].

### **3.2.4 Non Polymeric Coatings**

Non-polymeric options have also been explored for anticoagulant purposes. Metal–phenolic/catecholamine coated onto a stainless-steel rod exhibited good anticoagulant, antibacterial, and anti-inflammatory properties, thanks to the catalytic

release of nitrous oxide. The problem with this type of coating is that, while the coating continuously released nitrous oxide throughout testing, the reaction will not continue forever, and the potential duration of the reaction was not noted. Therefore, while it may work for short-term treatments, it is not yet suitable for coatings on implantable devices meant to last indefinitely [27].

A multifunctional coating, composed of hyaluronic acid and polydopamine, has also been examined, with the purpose of having good properties for anticoagulation, antihyperplasia, anti-inflammation and endothelialization. This is because these processes tend to contradict each other [28]. The coating was successful in showing good potential in all of the categories required, however, it has the same problem as the previous coating, as its anticoagulant properties are reliant on the release of nitrous oxide, which is not yet suitable for indefinite applications.

Of the non-polymeric options for anticoagulant coating, ultrananocrystalline diamond (UNCD) is easily one of the most fascinating and promising. Though it seems difficult to manufacture, this inexpensive coating has exhibited phenomenal anticoagulation properties. In comparison to the pyrolytic carbon, which is what most mechanical heart valves are composed of, both materials showed clot formation levels similar to a control, and the mechanical properties of UNCD are far superior to that of pyrolytic carbon for the intended application [29,30]. The main disadvantage of UNCD is that, although it is inexpensive, is the possible difficulty of production. The advantages and disadvantages of UNCD are compared to that of all other coatings described in Table 1.

### 3.2.5 Surface Modifications to Coatings

One of the key factors to consider when reviewing any material for potential use in anticoagulant coatings on implantable medical devices is the material's surface properties, as the material will be in direct contact with the blood. Surface properties include the material's hydrophobicity, protein adsorption, formability, and many others capable of being manipulated in numerous ways, including plasma treatment, chemical vapor deposition, and grafting. When deciding on potential materials for use in coatings for anticoagulation, suitable surface modifications should be evaluated in order to maximize the coating's potential effectiveness [30–34].

**Table 1.** Summary of current anticoagulant coatings.

Coating	Materials	Anticoagulation Mechanism	Approximate Effective Life	Pros	Cons	[Ref]
Drug-Eluting Stent Coating	Polymeric	Drug Release	6 to 12 Months	Proven Effectiveness	Only lasts a few months before dissolving	[18-20]
Heparin-Coated Film	Polymeric	Heparin	Up to 2 Months	Very Effective	Increases bleeding risk, chance of developing HIT	[18, 21]
Heparin-Mimicking/Heparin-Free Coating	Polymeric	Materials with plentiful carboxyl or sulfate groups	Varied, >2 Months	Effective, Low Health Risk	Not as effective as heparin due to lack of knowledge for heparin's effectiveness	[21]

Coating	Materials	Anticoagulation Mechanism	Approximate Effective Life	Pros	Cons	[Ref]
Polyurethane Films	Polymeric	Surface Properties	Varied	Very Effective, Highly Modifiable	Not enough research for this type yet, room for improvements	[22]
Polyurethane/Graphene/TC P Coating	Polymeric	N/A	N/A	Antibacterial Properties, Good Mechanical Properties	Becomes cytotoxic at 4 wt% graphene	[23]
Artificial Endothelium	Polymeric	Zwitterionic, Nitrous Oxide Release	Not enough long-term data	Very Effective	NO release may not last	[24]
Heparin/Graphene Coating	Polymeric	Heparin	Up to 2 Months	Effectiveness of Heparin and Antibacterial Properties of Graphene	Possibility for cytotoxicity, bleeding risk, and development of HIT	[25, 26]
Metal-Phenolic/Catecholamine Coating	Non-Polymeric	Nitrous Oxide Release	Not enough long-term data	Anticoagulant, Antibacterial, and Anti-Inflammatory Properties	NO release may not last	[27]
Hyaluronic Acid/Polydopamine Coating	Non-Polymeric	Nitrous Oxide Release	Not enough long-term data	Anticoagulant, Antihyperplasia, and Anti-Inflammatory Properties	NO release may not last	[28]
Ultranano crystalline Diamond Coating	Non-Polymeric	Surface Properties	>4 Weeks, not enough long-term data	Very Effective, Low Cost, Good Mechanical Properties	Seemingly difficult to produce	[29, 30]

### **3.2.6 Polyurethanes**

Of these coatings, one of the most promising options are polyurethanes (PUs). Polyurethanes are utilized extensively in various biomedical applications due to their excellent biocompatibility [35,36] and slow degradability [11,37,38]. They are produced using a variety of processes with structural components containing alternating soft segments (polyols) and hard segments (diisocyanates) at specific stoichiometric ratios, depending on the desired properties of the PUs [9]. A polyurethane is formed when a soft segment, containing hydroxyl groups (OH), and a hard segment, containing isocyanate groups (R-NCO), are combined together to form urethane linkages (-NHCO-) [10].

PUs are elastomers, meaning they have high tensile strength, are highly elastic, and have low crystallinity [39]. The combination of these properties and the excellent biocompatibility has led to a widespread research into its viability in biomedical applications. PU films have been shown to be an excellent option for various medical-grade applications, such as for protective coatings on implantable devices [40]. Another capability of PUs is drug delivery, where the polymer will either degrade to deliver drugs to a patient or have drugs eternally attached so that they will directly degrade into the body over time [41]. Similarly, PU films have displayed excellent anticoagulant properties, which makes them very practical as anticoagulant coatings to prolong the lifespan of implantable devices [22]. Others have synthesized PUs to create porous scaffolds that can be used to repair or replace damaged organs or tissues [42].

## Chapter 4: Materials and Methods

### 4.1 Materials

Polyethylene Glycol (PEG, MW 3400) was purchased in powder form from MP Biomedicals, LLC, and was chosen as the soft segment for its excellent biocompatibility. An 80/20 mixture of 2,4- and 2,6- Toluene Diisocyanate (TDI) was purchased in liquid form from VWR International, LLC, and was chosen as the hard segment for the mechanical properties it produces. N,N-Dimethylformamide (DMF) was purchased in liquid form from VWR International, LLC, and was used as the solvent to dissolve the PEG prior to synthesis. 1,4-Butanediol (BDO) was purchased in liquid form from VWR International, LLC, to be used as a chain extender.

### 4.2 Preparations of Polyurethane Commercial Films

In order to examine the viability of polyurethane films for use in anticoagulant coatings and the properties of different types and thicknesses of PU films, four sets of commercial films were purchased from Jiaying Inch Eco Materials Co., Ltd. (Zhejiang, China). These films included 0.06 mm and 0.1 mm polyester films (60ES and 100ES) and 0.06 mm and 0.2 mm polyether films (60ET and 200ET).

### 4.3 Synthesis of Polyurethane Samples

To synthesize each sample of polyurethane, a 15 wt% mixture of 1.2 g of PEG in 8 mL of DMF is first made and is mixed until all PEG is dissolved. The mixture is then placed inside a fume hood and into a water bath on a hot plate set to 70°C, and TDI is slowly added to the mixture. A magnetic stir bar is then added, and the solution is mixed

for up to 3 hours. The amount of TDI added and the time that the solution is mixed depends on the desired ratio of hard-to-soft segments of the polyurethane. 2 wt% of the chain extender BDO was added to some samples as well, after the TDI was able to mix. The laboratory setup for the synthesis process can be seen in Figure 2.

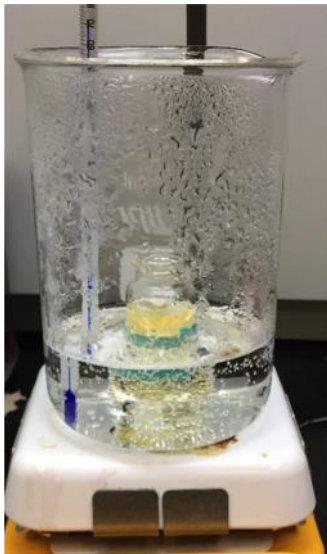


**Figure 2.** Laboratory setup for polyurethane synthesis, thermometer is included in beaker due to an inaccurate hot plate temperature.

Once the solution has been mixed and the release of  $\text{CO}_2$  from the reaction has ended, the solution is quickly poured into a flat mold and allowed to dry for 6 hours in order to create a film. To measure the yield mass of each ratio, the solutions were allowed to cool for 30 minutes, then poured into a beaker of water to precipitate the polymer, as shown in Figure 3. The solid polyurethane sample is removed from the water and allowed to dry overnight, then the yield mass is recorded.

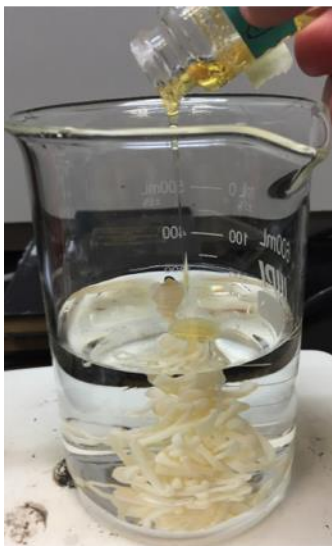


**Figure 3.** Visual representation of the precipitation process of the polyurethane samples.

#### **4.4 Fourier-Transform Infrared Spectroscopy (FTIR)**

The chemical structure of several polyurethane samples was analyzed using a Thermo Fisher Scientific Nicolet iS10 ATR-FTIR spectrophotometer (Waltham, MA, USA). The spectra were collected between 4000 and 650  $\text{cm}^{-1}$  with a resolution of 8  $\text{cm}^{-1}$ . Information for the peaks of the samples was obtained using OMNIC<sup>TM</sup> software.

#### **4.5 Differential Scanning Calorimetry (DSC)**

A Shimadzu DSC-50 (Kyoto, Japan) was utilized to examine the crystallinity, glass transition, and melting temperatures of the PU samples at a scanning rate of 20  $^{\circ}\text{C}/\text{min}$  between 25 and 200  $^{\circ}\text{C}$ . The weight of the specimens ranged between 6 and 10 mg. Three separate measurements were made for each sample, and the results were averaged.



#### **4.6 Thermal Gravimetric Analysis (TGA)**

Changes in the mass of the samples during thermal decomposition were explored through thermal gravimetric analysis using a Shimadzu TGA-50 Thermal Analyzer (Kyoto, Japan). The heating rate was 20 °C/min from 10 to 650 °C under N<sub>2</sub> gas with a flow rate of 30%. The weight of tested sample ranged between 15 and 18 mg. Three separate measurements were made for each sample, and the results were averaged.

#### **4.7 X-Ray Diffraction (XRD)**

The diffraction patterns of several PU samples were collected using a Rigaku R-Axis Spider<sup>TM</sup> (Tokyo, Japan). The x-ray source was produced from copper K $\alpha$  wavelength ( $\lambda = 1.541 \text{ \AA}$ ) at a 40 kV voltage and a current of 40 mA. The diffractometer was used in reflection mode. The XRD data was recorded at a resolution of  $2\theta = 0.05$  degree, from  $2\theta = 4$  to 40 degrees.

#### **4.8 Water Contact Angle and Water Absorption**

The surface hydrophilicity of several PU samples was determined by water contact angle measurements. A single droplet of phosphate-buffered saline (4  $\mu\text{L}$ ) was added to the surface of each sample, and the water contact angle was determined using ImageJ (National Institutes of Health, Bethesda, MD, USA) software. Three separate measurements were made for each sample, and the results were averaged.

Water absorption data was acquired by submerging 1" diameter disks of each PU sample into 3 mL of phosphate-buffered saline for up to 2 weeks. The submerged disks were placed in an incubator at 37°C under continuous shaking. At fixed time intervals,

the PU disks were removed from the saline and carefully dried to record the mass.

Percent weight change in water content was calculated using the equation below,

$$\%Weight\ Change = \frac{W_t - W_i}{W_i} \times 100\%$$

where  $W_i$  is the initial dry weight and  $W_t$  is the dry weight at each time interval. Three separate measurements were made for each sample, and the results were averaged.

#### **4.9 Mechanical Testing**

An Instron 3340 universal mechanical tester (Norwood, MA, USA) was used for the tensile testing of the PU samples, and testing was performed according to ASTM standard D882-18 (e.g.,  $23 \pm 2$  °C and  $50 \pm 5\%$  RH) [43]. The samples were cut into a dog-bone shape according to ASTM standard D1708-96 (22 mm in nominal length and 5 mm in width) [44]. Tensile tests were conducted at a strain rate of 0.01/s using a 100 N load cell. Stress-strain curves were generated using the raw load and displacement data obtained during testing. The elastic modulus was determined using the initial slope of the stress-strain curve after tensile testing. The tensile strength was obtained by dividing the maximum applied load to the cross-sectional area of the films. The elongation to failure was acquired from the stress strain curve at the strain (%) at which the specimen was split in two. Three separate measurements were made for each sample, and the results were averaged.

#### **4.10 Clotting Assays**

Two forms of in vitro activated partial thrombin time (APTT) assays were measured using an Organon Teknika Coag-A-Mate<sup>®</sup>XM (Durham, NC, USA). The

surfaces of each sample and all equipment used were washed using a mixture of typical household detergents and ethanol (75%) before each clotting experiment. Coagulation times were obtained as follows:

(1) 150  $\mu\text{L}$  of plasma was placed into a test tube along with 40  $\mu\text{L}$  of  $\text{CaCl}_2$ . The solution was thoroughly mixed and then applied to the surfaces of a glass plate (contact activation positive control) and each of the PU samples to be taken out at intervals of 0, 7, 10, 14, 17 and 22 minutes (contact time). At each interval, 100  $\mu\text{L}$  of the plasma/ $\text{CaCl}_2$  sample was then put into the Coag-A-Mate<sup>®</sup>XM and was activated immediately, utilizing this step as a warming process, with a time of 3 minutes. An additional 100  $\mu\text{L}$  of  $\text{CaCl}_2$  was added to the plasma/ $\text{CaCl}_2$  sample and clot formation was then recorded (clotting time). Three separate measurements were made for each sample, and the results were averaged.

(2) 700  $\mu\text{L}$  of plasma was placed into test tubes containing the control (glass beads) or shredded square PU samples with an estimated surface area equivalent to the glass beads. At fixed time intervals, 100  $\mu\text{L}$  of the plasma was removed from the test tube and 40  $\mu\text{L}$  of  $\text{CaCl}_2$  was added before being placed into the Coag-A-Mate<sup>®</sup>XM for activation. An additional 100  $\mu\text{L}$  of  $\text{CaCl}_2$  was added to the plasma/ $\text{CaCl}_2$  mixture and clot formation time was then recorded.

## Chapter 5: Results and Discussion

### 5.1 Commercial PU Films

#### 5.1.1 Appearance

Four samples of commercial PU films, 60ES, 100ES, 60ET, and 200ET, were physically examined by eye. The films, which can be seen in Figure 4, displayed no differences in their appearance and texture and were clear of noticeable flaws, such as cracks and air bubbles. The thicker films (i.e., 100ES and 200ET) were opaquer than their thinner counterparts (i.e., 60ES and 60ET). For the duration of the study, the films were stored under typical laboratory conditions (e.g.,  $23 \pm 2$  °C and  $50 \pm 5\%$  RH) and exhibited no signs of degradation and/or changes in appearance.



**Figure 4.** Physical appearance of the four commercial PU films: from left to right in the top wells, 200ET, 100ES, 60ES, and 60ET. The second row of 4 wells contains no PU films for comparison of the transparency of the PU films.

### 5.1.2 FTIR

FTIR spectroscopy is a nondestructive material characterization technique that can be utilized to quantitatively examine the chemical structure of polymers. For example, FTIR analysis has been used to study the physical state of pharmaceutical solids, including the amorphous/crystalline phases and the degree of crystallinity, based on the intensities of the characteristic peaks [45]. FTIR is also very useful when studying the urethane linkage ( $\text{-NHCO-}$ ) along with the composition of the soft segments in PU, such as ether ( $\text{R-O-R'}$ ) or ester ( $\text{R-COO-R'}$ ) [46,47]. Therefore, in this section, FTIR spectroscopy is utilized to determine the chemical structure of each of the PU samples. The FTIR spectra of the commercial PU films exhibited a strong peak at  $3330\text{ cm}^{-1}$ , which is assigned to the stretching vibration of N-H groups in the urethane linkage (Figure 5a) [48]. This N-H peak, which was noticeable for each PU samples, was somewhat overlapping with the O-H stretching peak at  $3400\text{ cm}^{-1}$ , which can typically be attributed to the presence of moisture in the air or within the sample. Nonetheless, the O-H stretching peak was generally broader than the N-H peak with less relative intensity when compared to other characteristic peaks in the  $1000\text{ cm}^{-1}$  to  $1600\text{ cm}^{-1}$  region [49]. Furthermore, the frequency of N-H stretching vibration tended to shift toward  $3400\text{ cm}^{-1}$  depending on the conformation of the urethane linkages with respect to one another under intermolecular hydrogen bonding. For example, the bands at  $3325\text{ cm}^{-1}$  and  $3313\text{ cm}^{-1}$  were associated with intramolecular hydrogen bonding of N-H and C=O within the urethane linkage, whereas the bands at  $3440\text{ cm}^{-1}$  and  $3451\text{ cm}^{-1}$  were attributed to the intermolecular hydrogen bonding [50]. Specifically, the intermolecular hydrogen bonds

in PU formed at the carbonyl groups in urethane linkage of the hard segments and/or at the carbonyl groups (ester) or oxygen (ether) groups in the soft segments [51]. For poly(ester-urethane), the competition of hydrogen bonding between the carbonyl groups of the hard segments and the soft segments determined the molecular configurations [52]. The ability to form hydrogen bonds was critical to the surface polarity and hemocompatibility of the PU as aliphatic PUs (all N–H groups are hydrogen bonded) tended to be more hydrophilic than aromatic PUs [53].

Further analysis of the FTIR spectra from the PU films suggested the characteristic peaks at  $1700\text{ cm}^{-1}$ ,  $1531\text{ cm}^{-1}$ , and  $1314\text{ cm}^{-1}$  due to C=O stretching vibration (amide I band), N–H bending vibration (amide II band) and C–N (amide III band) stretching vibration, respectively (Figure 5b) [48]. Additionally, the peak at  $1597\text{ cm}^{-1}$  indicated the skeletal vibration of C=C in the aromatic ring [54]. The evidence of the aromatic ring conformation in various PU samples was supported by the coupling peak at  $814\text{ cm}^{-1}$ , the most significant characteristic peak for out of plane bending vibration of C–H in 1,4-disubstituted aromatic ring [55]. This finding suggested the chemical structure of hard segment in the PU films consisted of aromatic polymer, such as diisocyanates [56]. In comparison, the absorbance between  $2930$  and  $2860\text{ cm}^{-1}$  (C–H stretching vibrations) coupled with the characteristic band patterns at  $1200$  and  $1100\text{ cm}^{-1}$  were the characteristic absorptions of C–O–C stretching vibrations, indicating the composition of esters and ethers, respectively, in the soft segments of the various PU samples [54].

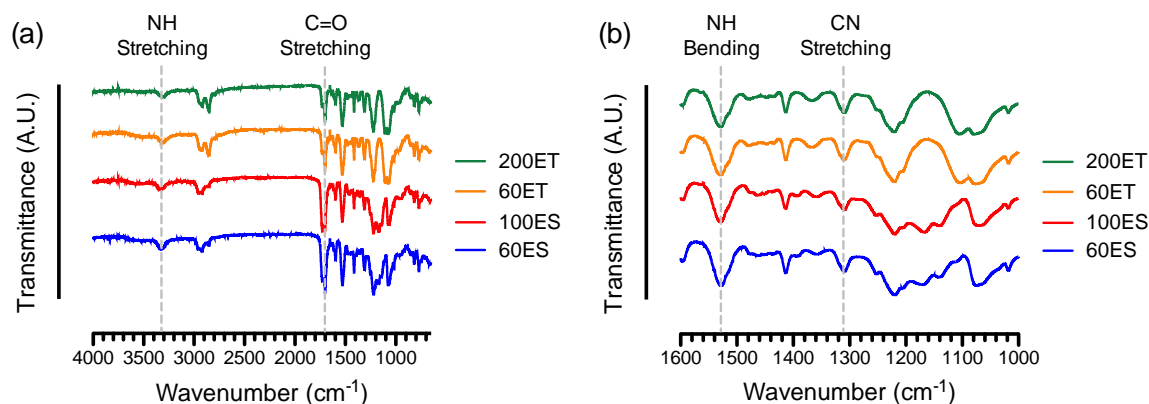


**Figure 5.** FTIR spectra of the various commercial PU films for: (a) wavenumbers from 650  $\text{cm}^{-1}$  to 4000  $\text{cm}^{-1}$  showing the characteristic peaks of N–H stretching vibration at around 3300  $\text{cm}^{-1}$  and C=O stretching vibration from amide I band at around 1700  $\text{cm}^{-1}$ ; (b) wavenumbers from 1000  $\text{cm}^{-1}$  to 1600  $\text{cm}^{-1}$  showing the characteristic peaks of N–H bending vibration from amide II band at around 1531  $\text{cm}^{-1}$  and C–N stretching vibration from amide III band at around 1314  $\text{cm}^{-1}$  that form the urethane linkage (–NHCO–).

### 5.1.3 DSC

According to the FTIR spectra, the commercial PU films consist of hard segments of diisocyanates and soft segments from esters and ethers, where the two segments are phase separated. DSC is useful when measuring the phase transition temperatures of the two phases. In particular, the glass transition temperature of the soft segments occurs at around  $-45^{\circ}\text{C}$  to  $-50^{\circ}\text{C}$ , and this thermal event is used to evaluate the purity of the soft phase [57,58]. Due to the limitations of available instruments, DSC measurements were conducted on the various PU films from  $25^{\circ}\text{C}$  to  $200^{\circ}\text{C}$  to focus on the thermal events above room temperature.

The representative DSC thermograms from the PU films are displayed in Figure 6. As shown in the figure, 200ET samples showed a thermal endotherm at  $55.1 \pm 1.3^{\circ}\text{C}$ , corresponding to melting of the soft segments. This thermal event was not visible in the other PU samples, suggesting that the 200ET comprised a different degree of crystallinity in the soft segments than the other PU samples [59]. This finding was in agreement with the supplier's manufacturing of PU samples where the 200ET samples were processed in a different batch.

As temperature increases, a small thermal endotherm was found at  $124.1 \pm 2.8^{\circ}\text{C}$ ,  $123.7 \pm 3.2^{\circ}\text{C}$ ,  $119.8 \pm 7.2^{\circ}\text{C}$ , and  $126.7 \pm 2.5^{\circ}\text{C}$  for 60ES, 100ES, 60ET, and 200ET, respectively. This thermal event is associated with the melting of hard segments that have long range ordering [58]. In particular, the 60ES and 100ES groups showed several other small thermal endotherms between  $120^{\circ}\text{C}$  and  $175^{\circ}\text{C}$ , suggesting that the poly(ester urethane) displayed a mixing of crystalline regions with various range of ordering [60,61]. Finally, the thermal endotherms between  $175^{\circ}\text{C}$  and  $200^{\circ}\text{C}$  were associated with the melting of the microcrystalline hard segments. In general, the DSC thermograms informed the melting of the hard and soft segments and the crystallinity of the various PU films. An increase in the crystallinity of the film increases the temperatures of the corresponding thermal events.



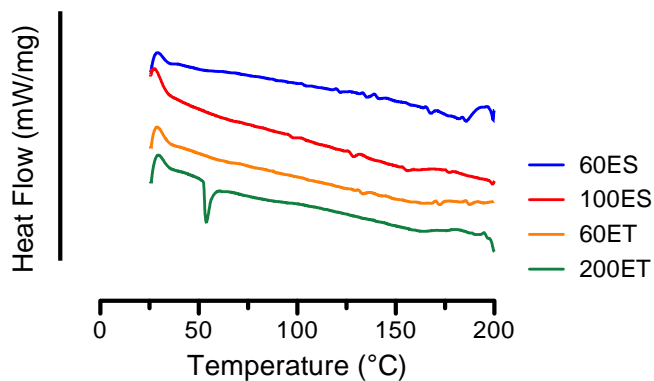


**Figure 6.** DSC thermograms of the various PU films from 25°C to 200°C, where a thermal endotherm at approximately 50°C for the 200ET groups corresponds to melting of the soft segments.

#### 5.1.4 TGA

Thermal stability of the various PU films was investigated by using TGA, and the percentage mass loss of various PU films at temperatures from 25°C to 650°C is shown in Figure 7a. The results show that the four types of PU films exhibited a similar mass loss profile with decomposition events began at approximately 276°C. Specifically, the average onset temperatures were  $355.0 \pm 2.1^\circ\text{C}$ ,  $359.3 \pm 1.6^\circ\text{C}$ ,  $337.1 \pm 2.0^\circ\text{C}$ , and  $354.2 \pm 2.1^\circ\text{C}$  for 60ES, 100ES, 60ET, and 200ET groups, respectively. The mass loss associated with the onset temperature was attributed to the dissociation of urethane linkages, including diisocyanates, alcohol, and amines [62]. In addition to the onset temperatures, there were negligible mass losses ( $< 0.1\%$ ) up to 250°C for the various PU films, suggesting that these samples contained very minimal water content [63].

The derivative of the mass loss in TGA profiles yields dTG curves, and the dTG curves are helpful in finding the peak decomposition temperatures along with the types of phase transitions during decomposition. As seen from the dTG curves shown in Figure 7b, 60ES and 100ES films both displayed a single peak located at an average temperature of  $406.1 \pm 13.9^\circ\text{C}$  and  $433.3 \pm 2.7^\circ\text{C}$ , respectively. In comparison, the 60ET and 200ET films displayed a two-stage decomposition process with the corresponding first peak located at an average temperature of  $385.6 \pm 5.0^\circ\text{C}$  and  $394.1 \pm 1.1^\circ\text{C}$  and the corresponding second peak located at an average temperature of  $437.8 \pm 1.6^\circ\text{C}$  and  $439.6 \pm 1.7^\circ\text{C}$ , respectively. The peak decomposition temperatures with their corresponding percentage mass losses for 60ES, 100ES, 60ET, and 200ET are listed in Table 2.

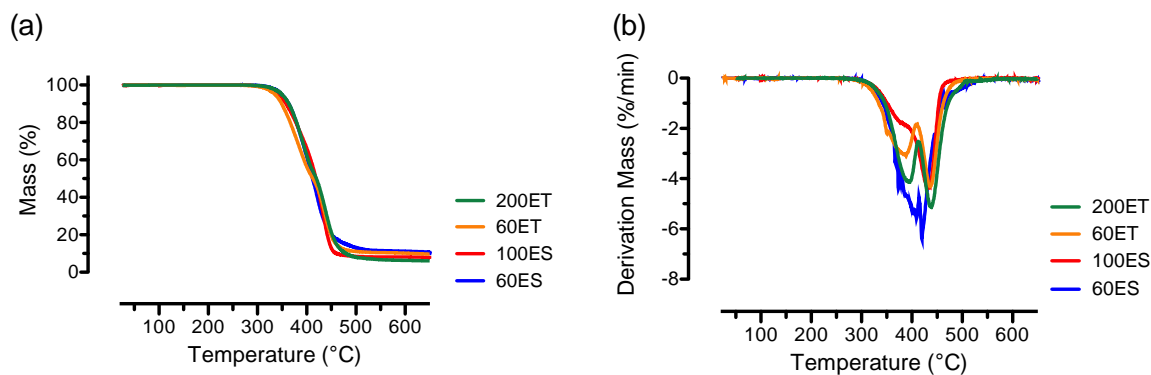


**Figure 7.** Thermal stability evaluations of the various PU films, showing (a) representative TGA curves on percentage mass loss with onset temperatures ranged between  $337^\circ\text{C}$  to  $355^\circ\text{C}$ ; (b) representative dTG curves where 60ES and 100ES groups exhibited single peak decomposition temperature and 60ES and 200ES groups displayed a two-step decomposition process.

**Table 2.** dTG temperatures and their corresponding percentage mass losses of the commercial PU films.

	First Step		Second Step	
	Temperature (°C)	Mass (%)	Temperature (°C)	Mass (%)
60ES	406.1 ± 13.9	52.2 ± 4.5	-	-
100ES	433.3 ± 2.7	33.2 ± 1.6	-	-
60ET	385.6 ± 5.0	68.1 ± 1.4	437.8 ± 1.6	32.2 ± 1.6
200ET	394.1 ± 1.1	69.0 ± 1.5	439.6 ± 1.7	34.3 ± 0.5

### 5.1.5 XRD

While infrared techniques are useful in observing the short-range molecular interactions, XRD provides information on the long-range ordering of the molecular chains. Additionally, XRD method is particularly suited for the determination of crystallinity [64] and chain orientation [65] in the segmented PU. Furthermore, depending on the amount of the hard and soft segments, phase separation may affect the structural regularity that leads to poor hemocompatibility.

The degree of crystallinity depends on the structure of diisocyanates as they form the backbone of the PU. As shown Figure 8, all samples showed a broad peak at  $2\theta = 20^\circ$ . The broad peak along with its small intensity suggested that the PU films were generally amorphous while carrying a small fraction of crystalline phase. The relatively low amount of the crystalline phase made the determination of the degree of crystallinity

difficult. Furthermore, aliphatic PUs typically had a sharp peak due to the aligned chain orientation while the aromatic PUs exhibited a much broader peak attributed to the amorphous structure [66]. Interestingly, the 60ET groups and the 100ES groups showed smaller peaks at  $2\theta = 21.8^\circ$  indicating some level of partial crystallization of the soft segment [66]. The results of the XRD testing is in agreement with the results from the FTIR analysis.

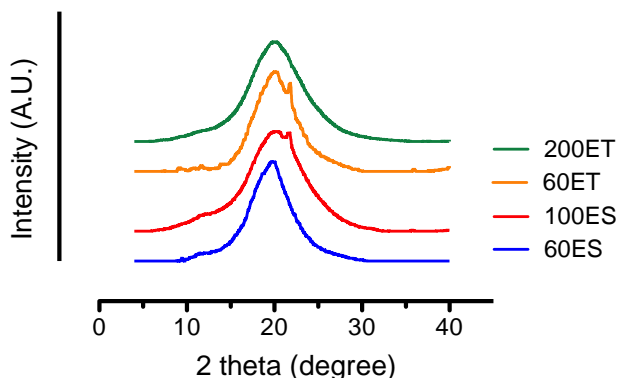


**Figure 8.** XRD patterns of the various PU films, showing a broad peak at  $2\theta = 20^\circ$  related to semicrystalline structure of the hard/soft segments in PUs. The small peaks at the shoulders of the 100ES and 60ET groups were attributed to the partial crystallization of the soft segments.

#### 5.1.6 Water Content Angle and Water Absorption

One of the most critical factors in determining hemocompatibility is a material's surface hydrophilicity/hydrophobicity, and these properties are found using the water contact angle experiment (Figure 9a). As shown in the representative image for each PU film, the water droplet formed a spherical shape due to the balanced net force between surface hydrophobicity of the film and the surface tension of the water droplet. The

results indicate that the surfaces of the PU films were hydrophobic with an average water contact angle of  $101.5 \pm 0.6$ ,  $96.4 \pm 1.5$ ,  $99.2 \pm 1.5$ , and  $114.0 \pm 1.8$  for 60ES, 100ES, 60ET, and 200ET groups, respectively. In comparison with a glass surface (control), which resulted in an average water contact angle of  $7.0 \pm 1.5$ , the notably high values of contact angles from the PU films ( $p < 0.05$ ) suggests that the PU samples were hydrophobic, which may be attributed to the aromatic configuration in the molecular structure (Figure 5).

Water absorption determines the amount of water intake of a material over a fixed time interval. High rates of water absorption may cause a change in surface hydrophobicity, which can affect the hemocompatibility of the material. If mass is lost, the test provides a useful insight into the material's degradation or dissolution. As shown by the results, all of the PU films exhibited a very minimal change in mass ( $< \pm 5\%$ ) over a 2-week period of observation (Figure 9b). Additionally, a short-term observation was performed to examine the water absorption behavior in the PU films (Figure 9b inset). Similar to the 2-week study, the PU films showed a minimal mass change ( $< \pm 5\%$ ) over 2h incubation period. The results suggest that there was a minimal to negligible change in mass of PU films, and as a result, the PU films were stable under physiological condition without noticeable changes in hydrophobicity as well as degradation behaviors.

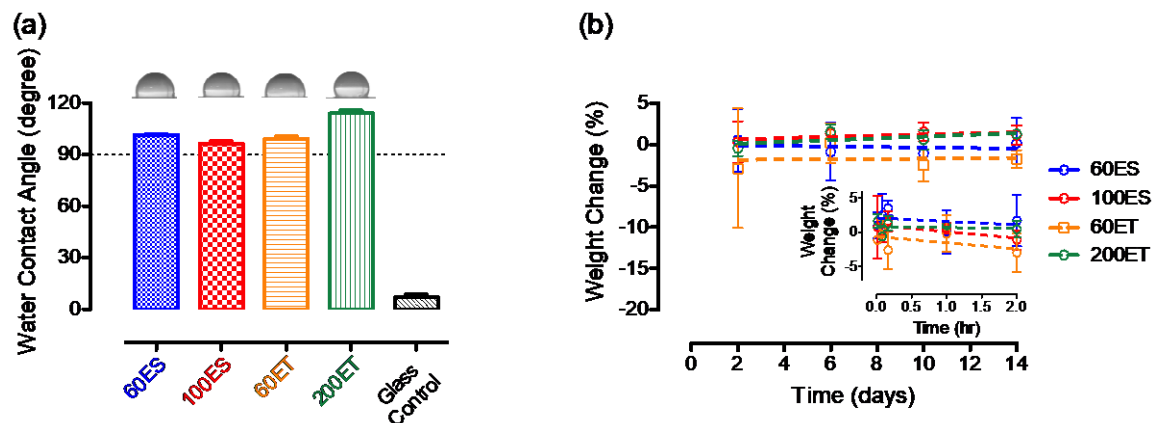


**Figure 9.** (a) Water contact angle study on the various commercial PU films comparing to a glass control. (b) Water absorption and/or degradation study on various commercial PU films over 14 days. Figure inset shows short-term study up to 2 h.

### 5.1.7 Mechanical Properties

Another critical factor when considering a material for the potential use of anticoagulation coatings on implantable devices is the material's mechanical properties. When introducing devices, such as cardiovascular stents, into the body, the shear force produced by the blood flow may cause coatings to degrade if they have inadequate strength. A more significant concern is that, once vascular stents are inserted into the body, they are required to expand and attach to the blood vessel. Therefore, coatings lacking sufficient elasticity are not suitable for anticoagulation applications.

The mechanical properties of the PU films were determined with tensile testing performed with an Instron materials tester with a force transducer under a constant strain rate in order to evaluate their mechanical properties. Stress-strain data acquired from the raw data during tensile testing was utilized to inform the chemical structure of the material [67]. A representative stress-strain curve for the 200ET film is shown in Figure

10a, and the stress-strain curves of the other PU films tested are similar to the representative curve.

An initial linear viscoelastic region can be seen on the stress-strain curve where the stress increase is proportional to the strain increase. After the linear viscoelastic region, stress increases minimally with increasing of strain (~ 400% strain). This region is associated with the unfolding of the soft segments. Since the PU components are more aromatic than aliphatic, the unfolding of the soft segments creates large amounts of strain. After the unfolding region, a strain-hardening region can be found where the significant stress increases are accompanied with the strain increase. This behavior is associated with the stretching of the molecular bonds that yields a much higher stress. The stress-strain curve shows that the PU films display a rubber-like behavior with three distinctive regions [68], as supported by the DSC data (Figure 6).

Information regarding the elastic modulus can be observed from the initial region, which is the slope at the beginning of the curve. The average moduli of the PU films are shown in Figure 10b, and are  $53.8 \pm 0.9$  MPa,  $20.0 \pm 1.0$  MPa,  $21.9 \pm 2.6$  MPa, and  $21.0 \pm 0.9$  MPa for the 60ES, 100ES, 60ET, and 200ET groups, respectively. The average modulus of the 60ES groups appears to be more than double that of the other films, suggesting that the material is intrinsically different than the others (e.g., crosslinking [69], hard/soft segment ratio [70], or types of hard/soft segments [71]).

Unfolding of the entangled molecular chain in the second region, primarily from the soft segments, can be obtained from the average elongation to failure. This property corresponds to the overall percentage of deformation that was applied to the material

before failure, and it is shown in Figure 10c. As shown in the figure, the average percentage elongation to failure was  $482.4 \pm 19.4\%$ ,  $746.3 \pm 37.9\%$ ,  $768.7 \pm 19.7\%$ , and  $794.9 \pm 22.0\%$  for the 60ES, 100ES, 60ET, and 200ET groups, respectively. These values match the finding from the elastic moduli, where the 60ES group displays a decrease in average percent elongation to failure of about 60% compared to the other films. This observation suggests that the 60ES groups are less elastic than other groups, suggesting the potential effects on crosslinking, different hard/soft segment ratios, or types of hard/soft segments used in the films.

The last region of the stress-strain curve is associated with the strain-hardening effect, and this phenomenon is quantified by the tensile strength of the material, which is found at the peak of the curve, the point at which the material fails. The average tensile strength of the PU films investigated is found in Figure 10d, and is  $46.7 \pm 3.7$  MPa,  $42.6 \pm 3.4$  MPa,  $26.9 \pm 3.4$  MPa, and  $42.9 \pm 1.8$  MPa for the 60ES, 100ES, 60ET, and 200ET films, respectively. While the 60ES, 100ES, and 200ET films display similar tensile strengths, the 60ET films appear to be noticeably weaker than the others ( $p < 0.05$ ). In a study, the decrease in tensile strength was attributed to the steric hindrance of the increased concentration of the side dimethyl and methyl groups [72]. Under constant strain, soft segment chains can be stretched and crystallized. This steric hindrance on the restriction of chain crystallization resulted in the decrease of the available sites for crosslinking and yielded a relatively low degree of microphase separation. This theory is supported by the DSC data of 60ET and 200 ET, where a melting of the soft segment was



found in 200 ET rather than the 60ET groups (Figure 6). Therefore, a decrease of tensile strength in the 60ET can be largely associated with this theory.

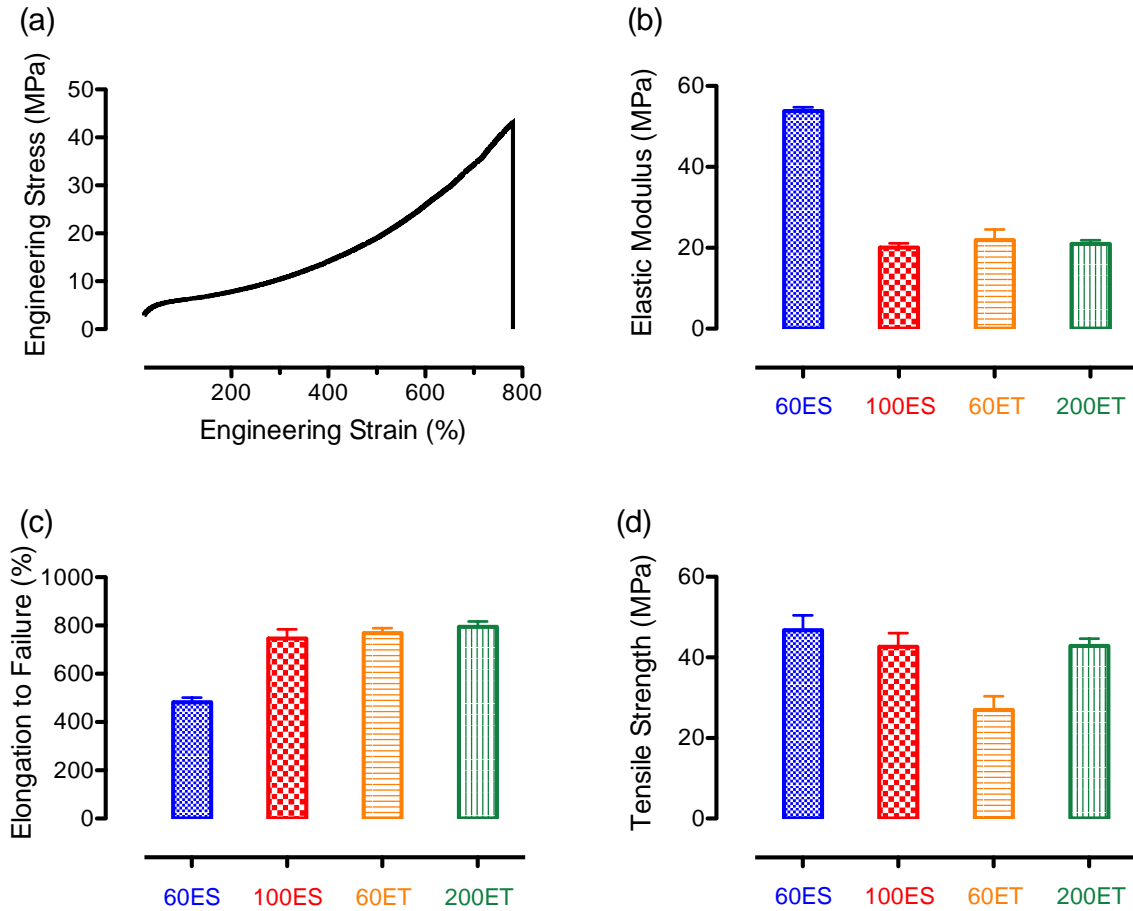


**Figure 10.** Mechanical properties of the various PU films, showing (a) a representative engineering stress-strain curve from 200ET groups; (b) average elastic moduli; (c) average elongation to failure; (d) average tensile strength.

### 5.1.8 Clotting Assays

As the intended purpose for the PU films is for use as anticoagulation coatings on implantable devices, the hemocompatibility of the PU films has to be evaluated. There are various studies showing that polyurethane is ideal for anticoagulant usage [73–75].

Therefore, in this section, the hemocompatibility of each PU film is evaluated by determining the rate of clotting when in contact with human blood plasma.

To find the clotting time, an in vitro clotting assay was initiated by placing a droplet of human blood plasma on the surfaces of the PU films in comparison with the surface of the glass control group (Figure 11a). Immediately after the contact with the PU surfaces (i.e., 0 min contact time), the clotting times were  $138 \pm 16$  s,  $169 \pm 4$  s,  $149 \pm 3$  s, and  $154 \pm 2$  s for 60ES, 100ES, 60ET, and 200ET films, respectively. These clotting times showed no statistical significance when compared to the glass control group ( $p > 0.05$ ). At 10 minutes of contact time, the clotting time for the glass control group was  $98 \pm 11$  s, whereas the clotting times for the PU films were  $160 \pm 17$  s,  $167 \pm 2$  s,  $145 \pm 19$  s, and  $163 \pm 4$  s for 60ES, 100ES, 60ET, and 200ET films, respectively. At the end of the assay (i.e., 22 min contact time), the plasma on the glass surface had clotted completely. In comparison, the clotting times of the PU films were  $131 \pm 67$  s,  $156 \pm 6$  s,  $154 \pm 20$  s, and  $162 \pm 7$  s for 60ES, 100ES, 60ET, and 200ET films, respectively. The results show that the PU films displayed excellent hemocompatibility with minimal change in the clotting time at fixed contact intervals up to 22 min.

In the first clotting assay, 40  $\mu$ L of  $\text{CaCl}_2$  were added to the plasma to activate the coagulation cascade by interacting with clotting factors, where the contact surface (e.g., the PU films or glass control) acted as the enabling substances [76]. Therefore, the concentration of the  $\text{CaCl}_2$  played an important role in evaluating the rate of clot formation. To see the effects of  $\text{CaCl}_2$  on the clotting time, an additional in vitro clotting assay was performed using 20 – 50  $\mu$ L of  $\text{CaCl}_2$  on 100ES, 200ET, and glass control

groups with 10 minutes of contact time (Figure 11b). Increasing calcium concentration from 20 to 50  $\mu\text{L}$  decreased the clotting times from  $143 \pm 3$  s to  $23 \pm 1$  s when the plasma was placed on the surface of glass control group. In contrast, the clotting times for 100ES and 200ET films were  $172 \pm 2$  s and  $167 \pm 3$  s at 20  $\mu\text{L}$  of  $\text{CaCl}_2$  and were  $167 \pm 5$  s and  $166 \pm 4$  s at 50  $\mu\text{L}$  of  $\text{CaCl}_2$ , respectively. Results suggest that calcium promoted clot formation, where the control group exhibited a dependence on the calcium concentration and the PU groups displayed an excellent degree of hemocompatibility.

The first in vitro clotting assay was performed under laboratory conditions where the plasma would dry out after 25 minutes. This assay limited the contact time to be no more than 22 minutes and combining with the  $\text{CaCl}_2$  concentration assay with a maximum level of  $\text{CaCl}_2$  in the 50  $\mu\text{L}$  to 60  $\mu\text{L}$  range, clotting due to the PU as an activating substance was unable to quantify. For this reason, a second in vitro clotting assay was performed where samples (plasma + activating substances) were placed into Eppendorf tubes that allowed for storage to up to 4 weeks or longer. At fixed time periods, a sample of plasma was taken out of the tube and placed into the coagulation analyzer to record the clotting time (Figure 11c). Using this assay, the clotting times of the PU films displayed a decrease of clotting time with a contact time that was 1000-fold longer than the glass control surface. Specifically, the clotting times were 63.3, 81.4, 45.8, and 48.9 s for 60ES, 100ES, 60ET, and 200ET films after 4 weeks of contact time (672 h), respectively. This result is notable because while the first clotting assay showed that the PU films displayed better hemocompatibility than the glass control, the length of contact time of the PU films was determined in the second in vitro clotting assay.

Various studies expressed that modified PUs displayed anticoagulant properties. For example, water-soluble chitosan/dextran sulfate was immobilized onto PU films and the clotting time was 670% longer than the native PU after 30 min of contact time [77]. Others added heparin into PU films to allow for slow heparin delivery [78]. Results showed that heparin-eluting PU films displayed clotting times greater than 200 s after 30 days of contact time. More importantly, the control PU films showed a clotting time of 46.8 s after the same contact time, and the results obtained with the commercial films are in agreement with the reported value. Furthermore, poly(ethylene glycol) monoacrylates (PEG-MAs) were grafted onto polycarbonateurethane films to increase the hydrophilicity of the films, which suppressed platelet adhesion to improve hemocompatibility [79]. In general, the results showed that the commercial PU films studied displayed excellent anticoagulant properties that were ideal for use as anticoagulation coatings on artificial organs and/or implantable devices to minimize clot formation.

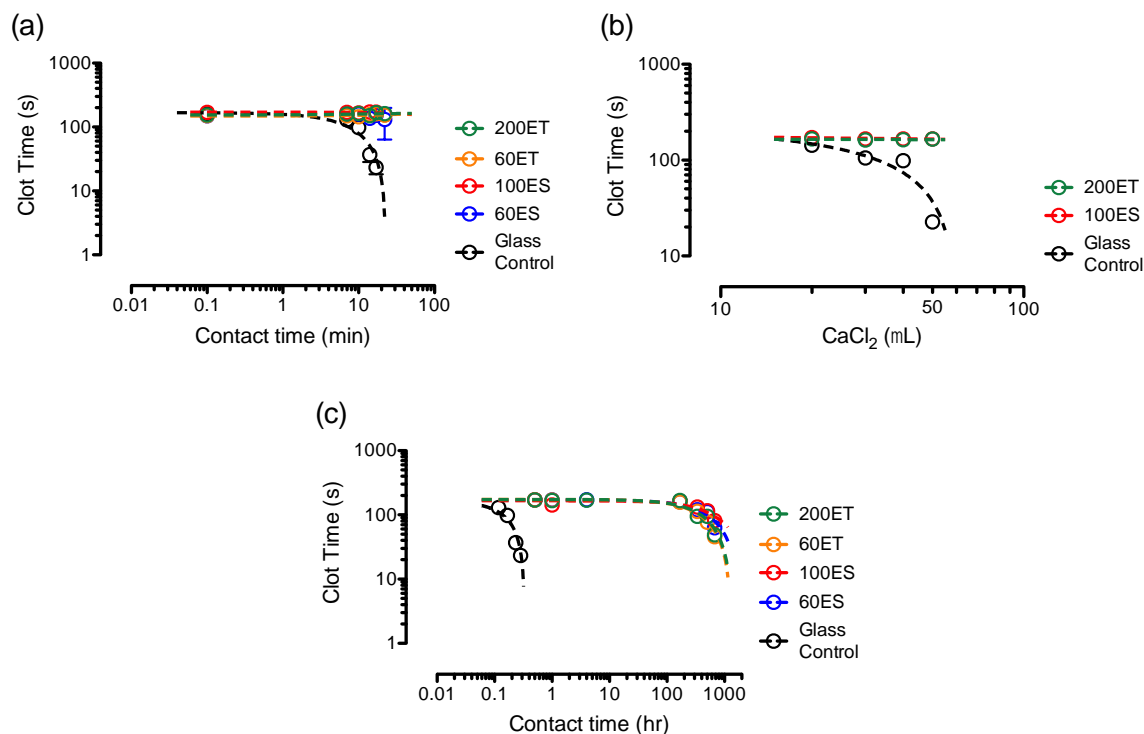


**Figure 11.** In vitro clotting assays on the various PU films in comparison with the glass control, showing (a) clotting assay (1) where human blood plasma were placed on the surface of the activating substances; (b) effects of  $\text{CaCl}_2$  concentrations on the clot times using clotting assay (1); (c) clotting assay (2) where human blood plasma and the activating substances were placed in an enclosure.

## 5.2 Films Synthesized In Lab

### 5.2.1 Synthesis

PU samples synthesized in the lab were carried out by step polymerization of PEG (soft segment) and TDI (hard segment) to form urethane linkages. In order to allow homogeneous mixture of the two polymer solutions, DMF was used to dissolve the PEG followed by slowly adding TDI solution into the PEG-containing DMF solvent. The resulting polymer mixture was slightly viscous with yellowish appearance and was free

of phase separation. After 3 hours of mixing at 75 °C, the polymer mixture was poured into DI-water to allow precipitation of the PU. The first two PU samples successfully precipitated in the lab in a trial-and-error effort based on the stoichiometric ratio of PEG-to-TDI consisted of the same PEG:TDI molar ratio (1:157).

After the successful precipitation of the PU samples from PEG:TDI mixture, the next several attempts were made using a 1:4 ratio; however, this mixture was unable to precipitate fully, suggesting a limitation on step polymerization efficiency between the PEG (soft segment) and the TDI (hard segment). To investigate the range of possible PEG:TDI ratios, four more samples were then successfully synthesized and precipitated, with ratios of 1:20, 1:40, 1:80, and 1:160 (PEG:TDI), to be used for testing and characterizations. The appearances of these precipitated samples can be seen in Figure 12 with variations in color due to the amount of PEG in the system.

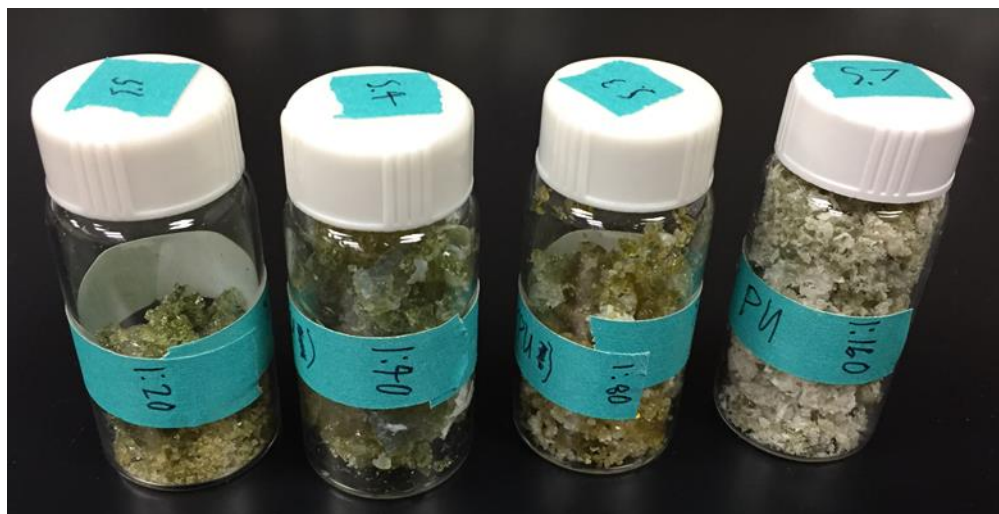


**Figure 12.** PU samples synthesized and precipitated in the lab at various PEG:TDI ratios, including 1:20, 1:40, 1:80, and 1:160, using step polymerization.

### 5.2.2 Yield Mass

PU synthesis using step polymerization in the lab was performed at a fixed volumetric amount of PEG (i.e., 15 wt% of PEG in 8 ml of DMF) where the amount of TDI increased from 1:20 to 1:160. The observation on the production of synthesized PU samples, shown in Figure 12, suggested an increase in the productivities of PU with increasing PEG:TDI ratios. A series of characterizations on the PU synthesis from PEG and TDI were performed on the reaction temperatures as well as PU yield in order to determine the process conditions for various PEG:TDI ratios.

During the synthesis of the initial four samples, it was discovered that the duration required for the solution mixture needed to be decreased with lower ratios of PEG:TDI. Over time, the viscosity of the lower ratios of PEG:TDI solution mixtures increased with several of the lower ratios of PEG:TDI samples thickening to the point that the stir bar was immobilized. While this effect was independent of solution's ability to be able to precipitate, the synthesis process of PU samples at lower ratios of PEG:TDI became more difficult with less ability to quality control the appearance of the PU samples. This lead to the creation of a standard curve for the heating time, shown in Figure 13, used for each ratio in order to reduce the chance for the sample to thicken too much for the precipitation process.

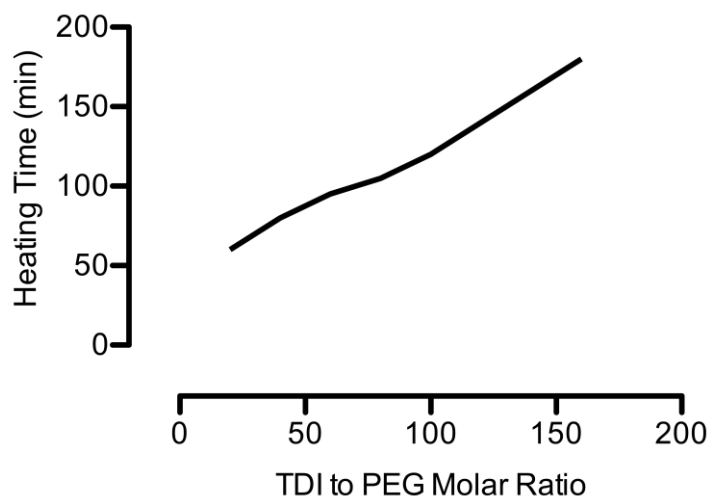


**Figure 13.** Standard heating times for the step polymerization of the PU samples from mixtures of PEG:TDI at different ratios.

After the creation of the standard curve for the heating time, synthesis of the PU samples was standardized from batch to batch to minimize sample differences within the same PEG:TDI ratio. Measurements on the yield mass of the produced PU sample at various ratio was evaluated and plotted in Figure 14. As expected, the yield mass increased at a steady rate from an average of 3.13 g to 11.1 g when the ratio of PEG:TDI increased from 1:20 to 1:80. However, as the ratio of PEG:TDI continued to increase from 1:80 to 1:160, the average yield mass in the precipitated PU only increased from 11.1 g to 13.3 g. These results suggested that synthesis of PU from PEG and TDI exhibited a linear region for the step polymerization followed by a decrease in the production rate that eventually reached stabilization of the process irrespective of the increase of TDI in the PEG:TDI mixture.



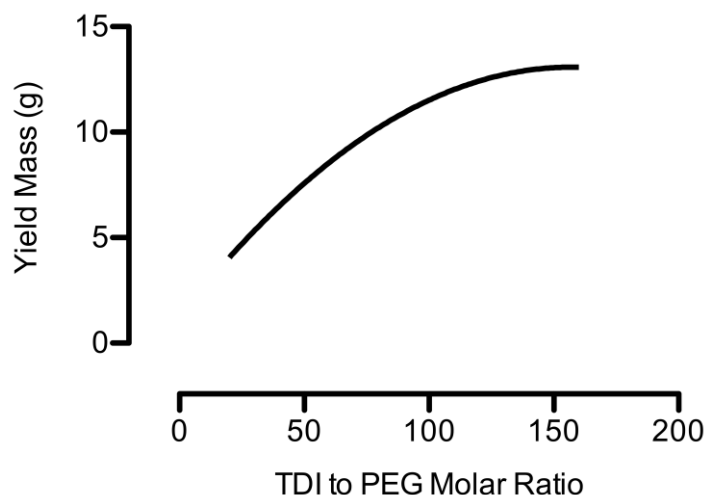


**Figure 14.** The relationship of yield mass obtained from the precipitated PU samples and the PEG:TDI ratios in the mixture for step polymerization.

### 5.2.3 Physical Appearance and Characteristics

The synthesized PU samples were then solvent cast into films for comparisons of their physical and mechanical properties with the commercial films. A total of eight sets of samples, including PEG:TDI ratios of 1:20, 1:40, 1:80, and 1:160 that were formulated with and without a chain extender (i.e., BDO), were prepared and evaluated first with their physical appearances.

The observations suggested that different ratios of PEG:TDI had an effect on the physical appearance and characteristics of the films as shown in Figure 15 illustrating the synthesized PU films at various PEG:TDI ratios without BDO. For example, the 1:20 films, shown in Figure 15a, were thinner and far more flexible than the other films. The 1:20 films tore easily while being removed from the molds, therefore requiring much more time and care. The 1:40 and 1:80 films, shown in Figure 15b and 15c respectively,

had very similar physical appearances and characteristics. The main difference between the two films was that the 1:80 films were slightly more brittle, which was expected due to a higher content of the hard segment (TDI) in the film as compared to the 1:40 films. The 1:160 films, shown in Figure 15d, were thick and brittle in addition to the appearance of several air bubbles throughout most of the samples.

The samples that contained BDO looked similar to their counterparts, and the main difference was that the 1:160 BDO films exhibited noticeably less air bubbles on the surface or within the sample itself as compared to those without BDO. For the duration of the study, the films were stored under typical laboratory conditions (e.g.,  $23 \pm 2$  °C and  $50 \pm 5\%$  RH) and exhibited no signs of degradation and/or changes in appearance.

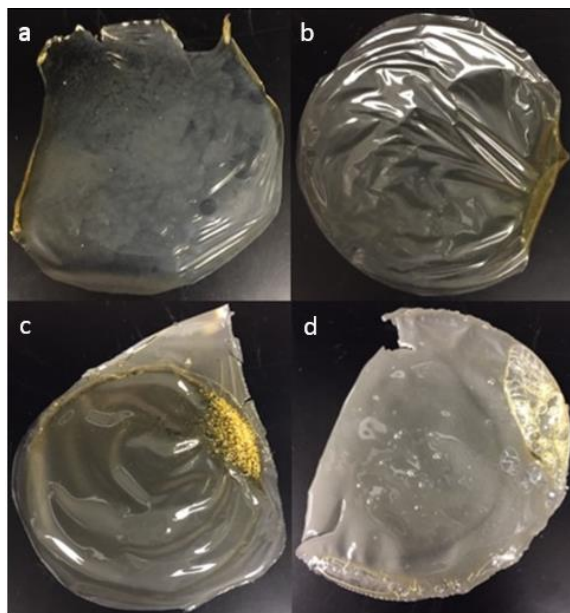


**Figure 15.** Physical appearance of the synthesized PU films at different ratios of PEG:TDI without the chain extender BDO: (a) 1:20, (b) 1:40, (c) 1:80, and (d) 1:160 (PEG:TDI) ratio.

### 5.2.4 FTIR Analysis

The FTIR spectra of the PU films without the inclusion of the chain extender (BDO) are shown in Figure 16. The lab-synthesized PU films exhibited characteristic peaks that were similar to those of the commercial films. For example, FTIR spectra of the lab-synthesized PU samples showed the characteristic peaks of N–H stretching vibration at around  $3300\text{ cm}^{-1}$  and C=O stretching vibration from amide I band at around  $1700\text{ cm}^{-1}$ . Also, the characteristic peaks of N–H bending vibration from amide II band at around  $1530\text{ cm}^{-1}$  and C–N stretching vibration from amide III band at around  $1310\text{ cm}^{-1}$  that form the urethane linkage ( $\text{--NHCO--}$ ) are shown. The main difference between the commercial films and the lab-synthesized samples is that the peak at around  $3300\text{ cm}^{-1}$  was not as defined for the lab-synthesized PU samples. This could be attributed to the presence of moisture, as the synthesis process of PU in the lab was not carried out under a nitrogen blanket that was generally recommended.

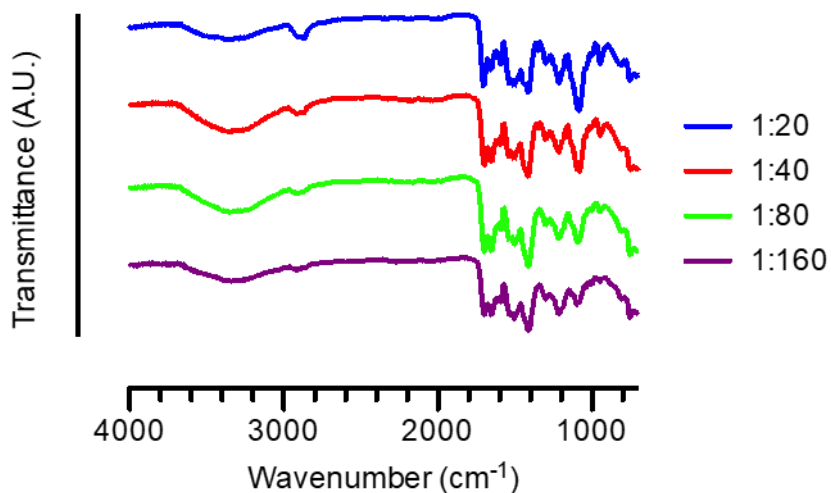


**Figure 16.** FTIR spectra of the synthesized PU samples for wavenumbers from  $700\text{ cm}^{-1}$  to  $4000\text{ cm}^{-1}$  showing the characteristic peaks of N–H stretching vibration at around  $3300$

$\text{cm}^{-1}$  and C=O stretching vibration from amide I band at around  $1700\text{ cm}^{-1}$ , as well as wavenumbers from  $1000\text{ cm}^{-1}$  to  $1600\text{ cm}^{-1}$  showing the characteristic peaks of N–H bending vibration from amide II band at around  $1531\text{ cm}^{-1}$  and C–N stretching vibration from amide III band at around  $1314\text{ cm}^{-1}$  that form the urethane linkage (–NHCO–).

### 5.2.5 Water Contact Angle Studies

The results of water contact angle tests on the lab-synthesized PU films, shown in Figure 17, indicated that the surfaces of the films were hydrophobic similar to the commercial films. In particular, the average water contact angle of lab-synthesized PU films without chain extender (BDO) decreased from  $112.3 \pm 4.7$ ,  $99.5 \pm 3.6$ ,  $99.6 \pm 5.1$ , to  $93.4 \pm 1.9$  as the TDI content increased from 1:20, 1:40, 1:80, and 1:160, respectively. In contrast, the average water contact angle of lab-synthesized PU films with chain extender (BDO) increased from  $96.6 \pm 4.3$ ,  $98.7 \pm 4.9$ ,  $96.9 \pm 2.0$ , to  $103.0 \pm 3.1$  as the TDI content increased from 1:20, 1:40, 1:80, and 1:160, respectively. In comparison with the glass surface (control) that was compared to the commercial PU films, which resulted in an average water contact angle of  $7.0 \pm 1.5$  (Figure 9a), the notably high values of water contact angles from the lab-synthesized PU films suggested that the PU samples were hydrophobic. The main difference between the films with and without the chain extender (BDO) was that the films with no BDO had slightly higher contact angles with the exception of the 1:160 films, though this could be attributed to the air bubbles on the surface of the 1:160 films without BDO creating an uneven surface. The higher angles could suggest that the films without BDO were slightly more hydrophobic than those with the chain extender, which could potentially exhibit anticoagulant ability.

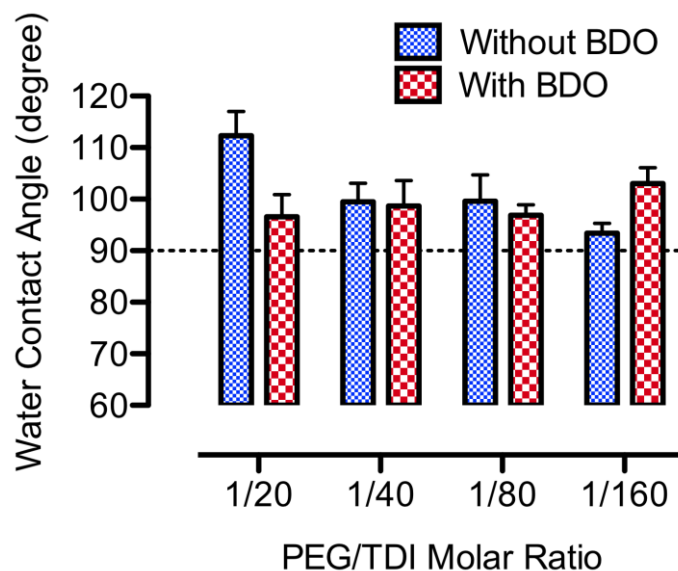


**Figure 17.** Water contact angle study on the various lab-synthesized PU films.

### 5.2.6 Water Absorption and Degradation Studies

Lab-synthesized PU samples, with and without chain extender (BDO), were incubated in DI-water at 37 °C for up to 2 weeks to evaluate water absorption behaviors and polymer degradation ability. During the incubation, all lab-synthesized PU films without chain extender (BDO) exhibited a very minimal change in mass ( $< \pm 5\%$ ) over a 2-hour period of observation (Figure 18a). The 1:20, 1:40, and 1:80 similarly displayed very minimal change in mass ( $< \pm 5\%$ ) over a 2-week period of observation (Figure 18b). However, the 1:160 films showed small changes in mass over the 2-week period and the 1:80 films lost about 10% of its mass before Day 2 during the 2-week incubation period. For these films, the results suggested that there was a minimal to negligible change in mass of the 1:20 and 1:40 PU films, and as a result, the PU films using these ratios were

stable under physiological condition without noticeable changes in hydrophobicity as well as degradation behaviors.

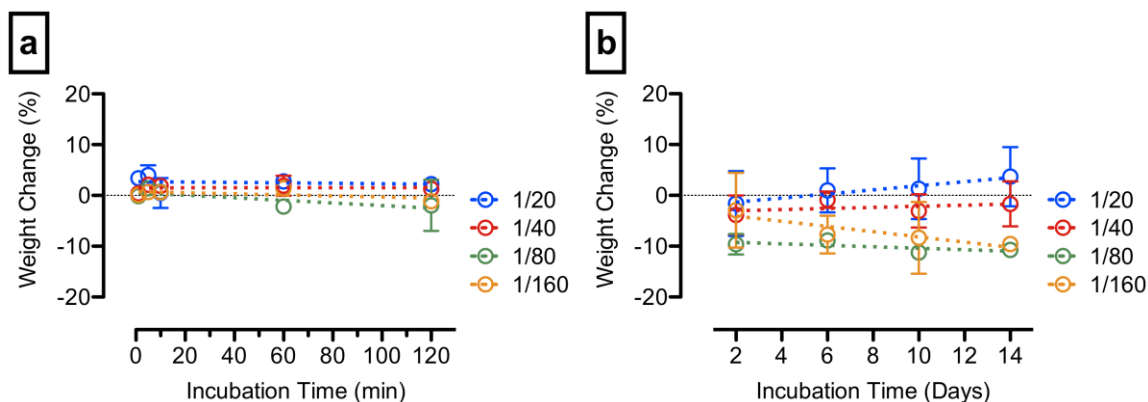


**Figure 18.** (a) Short-term water absorption and/or degradation study on the lab-synthesized PU films without BDO over 2 hours. (b) Long-term water absorption and/or degradation study on the lab-synthesized PU films without BDO over 14 days.

For the lab-synthesized PU samples with chain extender (BDO), all of the PU films exhibited a very minimal change in mass ( $< \pm 5\%$ ) over a 2-hour period of observation (Figure 19a). However, all of the PU films experienced some degree of change in mass ( $> \pm 5\%$ ) over a 2-week period of observation (Figure 19b). For these films, the results suggested that there was a significant change in mass of all PU films with BDO, and as a result, these were not stable under physiological condition.

The results of these tests show that, for very short-term applications, adding the chain extender will not cause a significant change in the water absorption or degradation properties of the PU films under physiological conditions. However, for applications that will exceed a few days, adding the chain extender to the PU films causes them to become

unstable under physiological conditions, which is not desirable for use in anticoagulation coatings on implantable biomedical devices.

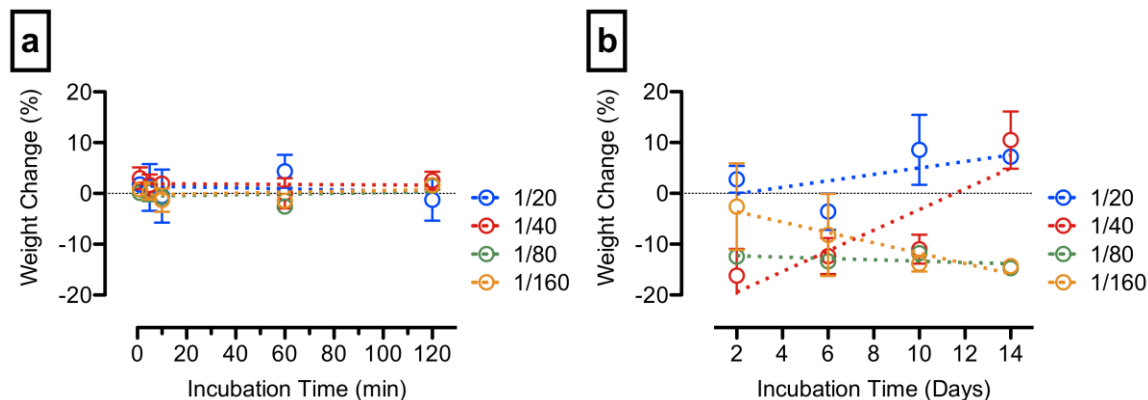


**Figure 19.** (a) Short-term water absorption and/or degradation study on the lab-synthesized PU films with BDO over 2 hours. (b) Long-term water absorption and/or degradation study on the lab-synthesized PU films with BDO over 14 days.

### 5.2.7 Mechanical Properties

Figure 20 shows the representative stress-strain curves for the lab-synthesized PU films without BDO. The 1:20 films shown in Figure 20a exhibited similar stress-strain behaviors to the commercial films. In general, the stress-strain curves of the 1:20 samples displayed a wider initial linear viscoelastic region followed by a shorter unfolding region ( $\sim 120\%$  strain), which was associated with the unfolding of the soft segment that creates a large amount of strain, than the commercial films. After the unfolding regions, the lab-synthesized 1:20 films showed a strain-hardening region, similar to the commercial films, that was associated with the stretching of molecular bonds that yields much higher increases in stress with the increasing strain. The stress-stain behaviors of other lab-

synthesized PU films were shown in Figure 20b. The 1:40 film exhibited an initial viscoelastic region and a very short unfolding region ( $\sim 14\%$  strain) before failure, which was expected due to the high content of the hard segment. This trend continued with the 1:80 and 1:160 films, which exhibited the initial viscoelastic region but fail at much smaller strain as these films became very brittle.

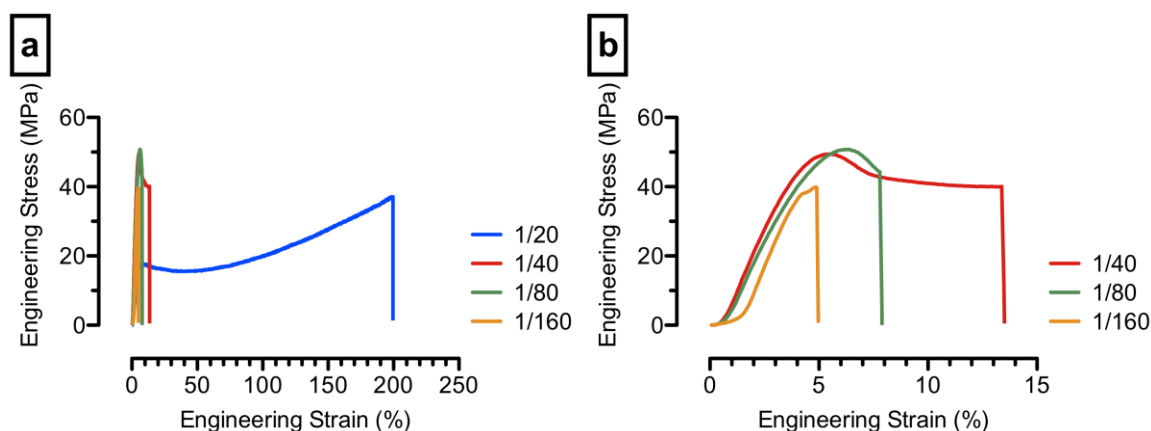


**Figure 20.** Representative engineering stress-strain curves of the various lab-synthesized PU film ratios without BDO: (a) All ratios, (b) 1:40, 1:80, and 1:160 films.

Figure 21 showed the representative stress-strain curves for the lab-synthesized PU films with chain extender (BDO). All of the ratios were virtually identical to those without BDO. The stress-strain curve of the 1:20 films with BDO shown in Figure 21a exhibited the characteristics of less semicrystalline than the counterpart due to the necking behavior near yielding. Nonetheless, the stress-strain behavior included a wide initial viscoelastic region, a short unfolding region ( $\sim 80\%$  strain), and a strain-hardening region. The stress-strain behaviors of other films were shown in Figure 21b, which displayed characteristics of brittle materials as the hard segment ratio increases. This



finding was similar to the films without the chain extender. Overall, the only significant difference between the films with and without the chain extender (BDO) was that the 1:20 films without BDO had a noticeably higher elongation to failure, which suggested that the addition of the chain extender reduced the flexibility of the PU to a small degree. This finding was consistent with other studies regarding the addition of a diol chain extender to PU containing TDI as the hard segment [80].

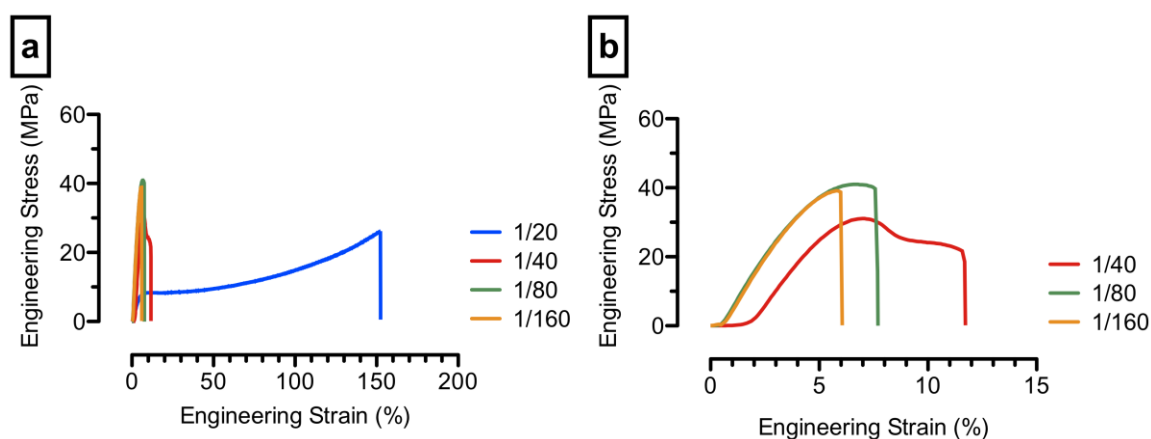


**Figure 21.** Representative engineering stress-strain curves of the various lab-synthesized PU film ratios with BDO: (a) All ratios, (b) 1:40, 1:80, and 1:160 films.

The average elastic moduli of the lab-synthesized PU films without BDO, shown in Figure 22a, were  $4.5 \pm 1.6$  MPa,  $13.9 \pm 2.5$  MPa,  $13.9 \pm 3.2$  MPa, and  $12.0 \pm 3.0$  MPa for the 1:20, 1:40, 1:80, and 1:160 films, respectively. Furthermore, the average elastic moduli of the lab-synthesized PU films with BDO were  $1.8 \pm 0.2$  MPa,  $10.3 \pm 3.5$  MPa,  $10.1 \pm 0.7$  MPa, and  $10.2 \pm 2.4$  MPa for the 1:20, 1:40, 1:80, and 1:160 films, respectively. The average elastic modulus of the 1:20 films were less than half that of the other ratios and were, therefore, far more flexible. Also, all of the films that contain BDO

have a noticeably lower elastic modulus than their non-BDO counterparts, which was consistent with other studies that suggested the decrease of elastic modulus and tensile strength due to the addition of BDO [81].

The average tensile strength of the lab-synthesized PU films without BDO, shown in Figure 22b, were  $35.2 \pm 1.7$  MPa,  $44.8 \pm 9.1$  MPa,  $43.7 \pm 6.2$  MPa, and  $37.9 \pm 1.8$  MPa for the 1:20, 1:40, 1:80, and 1:160 films, respectively. Furthermore, the average tensile strength of the lab-synthesized PU films with BDO were  $20.3 \pm 7.1$  MPa,  $32.9 \pm 10.6$  MPa,  $37.0 \pm 4.3$  MPa, and  $38.0 \pm 9.8$  MPa for the 1:20, 1:40, 1:80, and 1:160 films, respectively. For the films without BDO, the 1:40 and 1:80 were noticeably stronger than the 1:20 and 1:160 films. This was expected for the 1:20 due to the decreased content of the hard segments. In addition, decrease in strength for the 1:160 films was most likely associated with imperfections, such as air bubbles, along the surface of the films. The BDO films had a slightly lower tensile strength, which was consistent with other studies [81]. Tensile strength of the BDO containing samples increased in a more linear fashion than the non-BDO samples since the films contained less imperfections (e.g., air bubbles) along the surface of the films.

The average percentage elongation to failure of the lab-synthesized PU films without BDO, shown in Figure 22c, were  $230.7 \pm 47.9\%$ ,  $9.2 \pm 3.9\%$ ,  $5.7 \pm 2.3\%$ , and  $7.6 \pm 2.4\%$  for the 1:20, 1:40, 1:80, and 1:160 films, respectively. Furthermore, the average percentage elongation to failure of the lab-synthesized PU films with BDO were  $145.7 \pm 60.6\%$ ,  $8.3 \pm 3.0\%$ ,  $7.9 \pm 0.3\%$ , and  $8.6 \pm 4.4\%$  for the 1:20, 1:40, 1:80, and 1:160 films, respectively. These values matched the finding from the elastic moduli, where the 1:20

group displays a significant increase in average percent elongation to failure compared to the other films. This observation suggested that the 1:20 films were far more elastic than other groups, which was expected. The only significant difference, as noted earlier, was the noticeable decrease in elongation to failure of the 1:20 with BDO film compared to the 1:20 film without BDO, which was consistent with the addition of a diol chain extender to a TDI-based PU as shown in other studies [80].

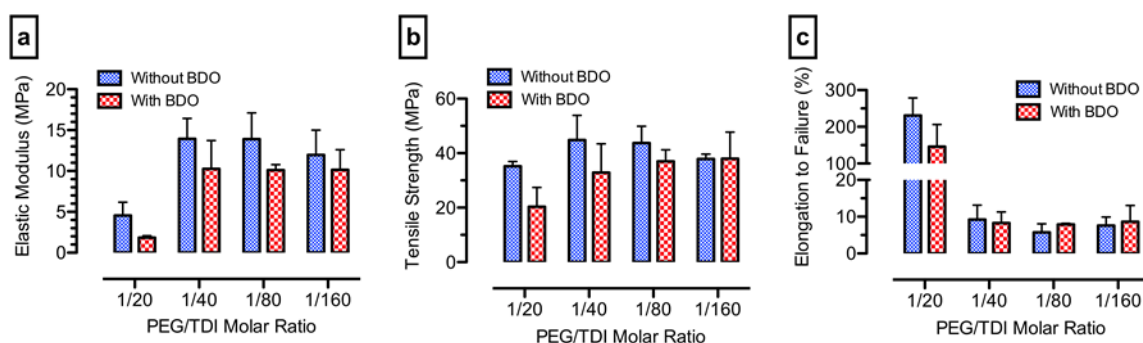


**Figure 22.** (a) Average elastic moduli of the various lab-synthesized PU film ratios, with and without BDO. (b) Average tensile strength of the various lab-synthesized PU film ratios, with and without BDO. (c) Average elongation to failure of the various lab-synthesized PU film ratios, with and without BDO.

### 5.2.8 Comparison to Commercial Films

As all of the other lab-synthesized films were shown to be unstable under physiological conditions, the 1:20 and 1:40 films without BDO are the only films suitable for use in anticoagulant coatings. Table 3 shows a comparison of the properties of these films compared to the commercial films. Both lab films had similar tensile strengths to the commercial films, however, both had lower elastic moduli. The 1:40 film had a

significantly lower elongation to failure, while the 1:20 film had the closest value to those of the commercial films, though it was still much lower. With modifications to the lab films, it should be possible to optimize their properties to get them closer to those of the commercial films.

**Table 3.** Comparison of mechanical properties of the commercial films to the lab films.

Films	Elastic Modulus (MPa)	Tensile Strength (MPa)	Elongation to Failure (%)
1:20 No BDO	$4.5 \pm 1.6$	$35.2 \pm 1.7$	$230.7 \pm 47.9$
1:40 No BDO	$13.9 \pm 2.5$	$44.8 \pm 9.1$	$9.2 \pm 3.9$
60ES	$53.8 \pm 0.9$	$46.7 \pm 3.7$	$482.4 \pm 19.4$
100ES	$20.0 \pm 1.0$	$42.6 \pm 3.4$	$746.3 \pm 37.9$
60ET	$21.9 \pm 2.6$	$26.9 \pm 3.4$	$768.7 \pm 19.7$
200ET	$21.0 \pm 0.9$	$42.9 \pm 1.8$	$794.9 \pm 22.0$

## Chapter 6: Conclusions and Future Work

In this work, the viability of polyurethane films for potential use as anticoagulation coatings on implantable medical devices was examined. Four commercial films, two polyester urethane films and two polyether urethane films, of various thicknesses and shore hardness were purchased and tested to determine their chemical, thermal, physical, and mechanical properties, as well as evaluating their anticoagulant abilities. The FTIR analysis of the commercial PU films showed the presence of characteristic chemical bonds, confirming that the films included both polyester- and polyether-urethanes. However, the specific materials used to synthesize the commercial films is still unknown.

The DSC and TGA testing displayed the thermal stability and properties of the films. XRD analysis, along with DSC, displayed the crystallinity of the films, as well as the chain orientation. The water contact angle results exhibited the hydrophobicity of the films and the absorption/degradation tests showed that the films experienced no significant change in mass. The mechanical testing displayed the high degree of elasticity of the films and great tensile strength. The elasticity of the films, along with their lack of degradation, means that the films fulfill the necessary mechanical properties for use in applications like stent coatings. Finally, the results of the second clotting assay showed that the films are capable of delaying the onset of clot formation to a significant degree.

The results gathered through all of the testing performed on the commercial films showed that polyurethane films had excellent thermal and physico-mechanical properties for use in anticoagulant coatings and are capable of increasing contact time by a

thousand-fold compared to a control. However, the lack of knowledge regarding the specific composition and structure of the commercial films means that vital properties, such as the long-term biocompatibility of the films, could not be easily determined or modified. Therefore, samples were synthesized in-house to be used for further research. The samples were synthesized with a range of different hard-to-soft segment ratios in order to optimize the properties of the final products.

PEG and TDI were chosen as the soft and hard segments, based on the biocompatibility of PEG and the mechanical properties of TDI, and samples of several ratios were successfully synthesized, as confirmed from the FTIR results. Several ratios were used in order to find which ratio produced a film with optimal properties for the intended purpose. The hard-to-soft segment ratios chosen were 1:20, 1:40, 1:80, and 1:160, based on initial attempts to synthesize and precipitate the polyurethane, as well as to examine how these ratios would affect the physico-mechanical properties of the films produced. Another set of films with these ratios that included BDO as a chain extender was also synthesized to examine how it further affected the properties of the films

While it was expected that the ratios would affect the physico-mechanical properties of the films, it was noted during the synthesis process that yield mass, physical appearance, and the mixing time necessary when preparing the polymer were also affected. Higher ratios of the hard-to-soft segments had a higher yield mass and required a longer mixing time. Also, the higher ratio films, mainly the 1:160 group, caused several issues during the synthesis process, as air bubbles and cracking was a constant problem with these films.

Water contact angle testing performed on the lab-synthesized films showed that all were hydrophobic. The water absorption/degradation study on these films displayed that most of the films experienced a significant change in weight over a two-week period and were, therefore, hydrolytically unstable under physiological conditions. The only films that exhibited no significant mass change were the 1:20 and 1:40 films that did not contain BDO. The mechanical testing results showed that all of the films exhibited great tensile strength, but the 1:20 films were, by far, the most elastic.

For anticoagulation coatings on implantable biomedical devices, the 1:20 PU films without BDO exhibited the best physico-mechanical properties compared to the other ratios. While the 1:40 ratio also exhibited viable properties for the application, it lacked the elasticity necessary for certain devices, such as cardiac stents that have to expand. All other ratios experienced too much hydrolytic instability under physiological conditions to be considered.

For future work, it is suggested to perform clotting assays and degradation studies over a much longer time interval in order to evaluate the effective lifetime of the 1:20 films, as well as to determine if cytotoxicity becomes an issue due to the aromatic components in the films. It is also suggested to explore and evaluate different surface modifications that could help prevent hydrolytic degradation and to further lengthen clotting times.

## References

- [1] What is Venous Thromboembolism (VTE)?, Www.Heart.Org. (n.d.).  
<https://www.heart.org/en/health-topics/venous-thromboembolism/what-is-venous-thromboembolism-vte> (accessed October 3, 2019).
- [2] Cost of Blood Clot Treatment - Consumer Information, (n.d.).  
<https://health.costhelper.com/blood-clots.html> (accessed October 3, 2019).
- [3] FastStats, (2019). <https://www.cdc.gov/nchs/fastats/heart-disease.htm> (accessed October 3, 2019).
- [4] Over 1.8 Million Stents Implanted per Year in the U.S., IData Res. (2018).  
<https://idataresearch.com/over-1-8-million-stents-implanted-per-year-in-the-u-s/> (accessed October 3, 2019).
- [5] Cost of a Heart Stent - Consumer Information, (n.d.).  
<https://health.costhelper.com/stents.html> (accessed October 3, 2019).
- [6] Your Guide to Preventing and Treating Blood Clots, (2009).  
<https://www.ahrq.gov/patients-consumers/prevention/disease/bloodclots.html> (accessed October 3, 2019).
- [7] M. Small, A. Faglie, A. Craig, M. Pieper, V. Fernand Narcisse, P. Neuenschwander, S.-F. Chou, M. Small, A. Faglie, A.J. Craig, M. Pieper, V.E. Fernand Narcisse, P.F. Neuenschwander, S.-F. Chou, Nanostructure-Enabled and Macromolecule-Grafted Surfaces for Biomedical Applications, *Micromachines*. 9 (2018) 243.  
<https://doi.org/10.3390/mi9050243>.



- [8] A. Wilson, P. Neuenschwander, S.-F. Chou, Engineering Approaches to Prevent Blood Clotting from Medical Implants, *Arch. Biomed. Eng. Biotechnol.* 1 (2019). <https://doi.org/10.33552/ABEB.2018.01.000510>.
- [9] D. Sarkar, J.-C. Yang, S.T. Lopina, Structure-property relationship of L-tyrosine-based polyurethanes for biomaterial applications, *J. Appl. Polym. Sci.* 108 (2008) 2345–2355. <https://doi.org/10.1002/app.27637>.
- [10] M. Marzec, J. Kucińska-Lipka, I. Kalaszczyńska, H. Janik, Development of polyurethanes for bone repair, *Mater. Sci. Eng. C.* 80 (2017) 736–747. <https://doi.org/10.1016/j.msec.2017.07.047>.
- [11] S. Oprea, Dependence of fungal biodegradation of PEG/castor oil-based polyurethane elastomers on the hard-segment structure, *Polym. Degrad. Stab.* 95 (2010) 2396–2404. <https://doi.org/10.1016/j.polymdegradstab.2010.08.013>.
- [12] P.F. Neuenschwander, J. Jesty, Blood Coagulation, *Encycl. Life Sci.* (2011). <https://doi.org/10.1002/9780470015902.a0000904.pub3>.
- [13] P.F. Neuenschwander, S.R. Williamson, A. Nalian, K.J. Baker-Deadmond, Heparin Modulates the 99-Loop of Factor IXa: *EFFECTS ON REACTIVITY WITH ISOLATED KUNITZ-TYPE INHIBITOR DOMAINS*, *J. Biol. Chem.* 281 (2006) 23066–23074. <https://doi.org/10.1074/jbc.M603743200>.
- [14] S.A. Smith, R.J. Travers, J.H. Morrissey, How it all starts: initiation of the clotting cascade, *Crit. Rev. Biochem. Mol. Biol.* 50 (2015) 326–336. <https://doi.org/10.3109/10409238.2015.1050550>.

- [15] T.A. Moran, C.S. Viele, Normal Clotting, *Semin. Oncol. Nurs.* 21 (2005) 1–11.  
<https://doi.org/10.1016/j.soncn.2005.10.014>.
- [16] R. Gbyli, A. Mercaldi, H. Sundaram, K.A. Amoako, Achieving Totally Local Anticoagulation on Blood Contacting Devices, *Adv. Mater. Interfaces.* 5 (2018) 1700954. <https://doi.org/10.1002/admi.201700954>.
- [17] X. Wang, Overview on Biocompatibilities of Implantable Biomaterials, *Adv. Biomater. Sci. Biomed. Appl.* (2013). <https://doi.org/10.5772/53461>.
- [18] Polymer coatings for biocompatibility and reduced nonspecific adsorption | Elsevier Enhanced Reader, in: *Funct. Cardiovasc. Stents*, Woodhead Publishing, 2018: pp. 155–198. <https://doi.org/10.1016/B978-0-08-100496-8.00009-3>.
- [19] R. Doshi, J. Shah, V. Jauhar, D. Decter, R. Jauhar, P. Meraj, Comparison of drug eluting stents (DESs) and bare metal stents (BMSs) with STEMI: who received BMS in the era of 2nd generation DES?, *Heart Lung.* 47 (2018) 231–236.  
<https://doi.org/10.1016/j.hrtlng.2018.02.004>.
- [20] A. Kalra, H. Rehman, S. Khera, B. Thyagarajan, D.L. Bhatt, N.S. Kleiman, R.W. Yeh, New-Generation Coronary Stents: Current Data and Future Directions, *Curr. Atheroscler. Rep.* 19 (2017) 14. <https://doi.org/10.1007/s11883-017-0654-1>.
- [21] H. Wang, X. Shi, A. Gao, H. Lin, Y. Chen, Y. Ye, J. He, F. Liu, G. Deng, Heparin free coating on PLA membranes for enhanced hemocompatibility via iCVD, *Appl. Surf. Sci.* 433 (2018) 869–878. <https://doi.org/10.1016/j.apsusc.2017.10.123>.
- [22] C. Chi, B. Sun, N. Zhou, M. Zhang, X. Chu, P. Yuan, J. Shen, Anticoagulant polyurethane substrates modified with poly(2-methacryloyloxyethyl

- phosphorylcholine) via SI-RATRP, *Colloids Surf. B Biointerfaces*. 163 (2018) 301–308. <https://doi.org/10.1016/j.colsurfb.2018.01.005>.
- [23] B. Szaraniec, K. Pielichowska, E. Pac, E. Menaszek, Multifunctional polymer coatings for titanium implants, *Mater. Sci. Eng. C*. 93 (2018) 950–957. <https://doi.org/10.1016/j.msec.2018.08.065>.
- [24] K.A. Amoako, H.S. Sundaram, A. Suhaib, S. Jiang, K.E. Cook, Multimodal, Biomaterial-Focused Anticoagulation via Superlow Fouling Zwitterionic Functional Groups Coupled with Anti-Platelet Nitric Oxide Release, *Adv. Mater. Interfaces*. 3 (2016) 1500646. <https://doi.org/10.1002/admi.201500646>.
- [25] R. Biran, D. Pond, Heparin coatings for improving blood compatibility of medical devices, *Adv. Drug Deliv. Rev.* 112 (2017) 12–23. <https://doi.org/10.1016/j.addr.2016.12.002>.
- [26] C.-J. Pan, L.-Q. Pang, F. Gao, Y.-N. Wang, T. Liu, W. Ye, Y.-H. Hou, Anticoagulation and endothelial cell behaviors of heparin-loaded graphene oxide coating on titanium surface, *Mater. Sci. Eng. C*. 63 (2016) 333–340. <https://doi.org/10.1016/j.msec.2016.03.001>.
- [27] X. Li, P. Gao, J. Tan, K. Xiong, M.F. Maitz, C. Pan, H. Wu, Y. Chen, Z. Yang, N. Huang, Assembly of Metal–Phenolic/Catecholamine Networks for Synergistically Anti-Inflammatory, Antimicrobial, and Anticoagulant Coatings, *ACS Appl. Mater. Interfaces*. 10 (2018) 40844–40853. <https://doi.org/10.1021/acsami.8b14409>.
- [28] F. Wu, J. Li, K. Zhang, Z. He, P. Yang, D. Zou, N. Huang, Multifunctional Coating Based on Hyaluronic Acid and Dopamine Conjugate for Potential Application on

Surface Modification of Cardiovascular Implanted Devices, *ACS Appl. Mater.*

*Interfaces*. 8 (2016) 109–121. <https://doi.org/10.1021/acsami.5b07427>.

- [29] H. Zeng, R. Jarvik, G. Catausan, N. Moldovan, J. Carlisle, Diamond coated artificial cardiovascular devices, *Surf. Coat. Technol.* 302 (2016) 420–425.

<https://doi.org/10.1016/j.surfcoat.2016.06.030>.

- [30] H. Zeng, W. Yin, G. Catausan, N. Moldovan, J. Carlisle, Ultrananocrystalline diamond integration with pyrolytic carbon components of mechanical heart valves, *Diam. Relat. Mater.* 61 (2016) 97–101.

<https://doi.org/10.1016/j.diamond.2015.11.020>.

- [31] Y. Ikada, Surface modification of polymers for medical applications, *Biomaterials*. 15 (1994) 725–736. [https://doi.org/10.1016/0142-9612\(94\)90025-6](https://doi.org/10.1016/0142-9612(94)90025-6).

- [32] D.L. Elbert, J.A. Hubbell, *Surface Treatments of Polymers for Biocompatibility*, (n.d.) 31.

- [33] X. Liu, P.K. Chu, C. Ding, Surface modification of titanium, titanium alloys, and related materials for biomedical applications, *Mater. Sci. Eng. R Rep.* 47 (2004) 49–121. <https://doi.org/10.1016/j.mser.2004.11.001>.

- [34] P.K. Chu, J.Y. Chen, L.P. Wang, N. Huang, Plasma-surface modification of biomaterials, *Mater. Sci. Eng. R Rep.* 36 (2002) 143–206.

[https://doi.org/10.1016/S0927-796X\(02\)00004-9](https://doi.org/10.1016/S0927-796X(02)00004-9).

- [35] S.-H. Hsu, Y.-C. Kao, Biocompatibility of poly(carbonate urethane)s with various degrees of nanophase separation, *Macromol. Biosci.* 5 (2005) 246–253.

<https://doi.org/10.1002/mabi.200400163>.

- [36] S. Miao, L. Sun, P. Wang, R. Liu, Z. Su, S. Zhang, Soybean oil-based polyurethane networks as candidate biomaterials: Synthesis and biocompatibility, *Eur. J. Lipid Sci. Technol.* 114 (2012) 1165–1174. <https://doi.org/10.1002/ejlt.201200050>.
- [37] A.B. Mathur, T.O. Collier, W.J. Kao, M. Wiggins, M.A. Schubert, A. Hiltner, J.M. Anderson, In vivo biocompatibility and biostability of modified polyurethanes, *J. Biomed. Mater. Res.* 36 (1997) 246–257. [https://doi.org/10.1002/\(SICI\)1097-4636\(199708\)36:2<246::AID-JBM14>3.0.CO;2-E](https://doi.org/10.1002/(SICI)1097-4636(199708)36:2<246::AID-JBM14>3.0.CO;2-E).
- [38] B.R. Barrioni, S.M. de Carvalho, R.L. Oréfice, A.A.R. de Oliveira, M. de M. Pereira, Synthesis and characterization of biodegradable polyurethane films based on HDI with hydrolyzable crosslinked bonds and a homogeneous structure for biomedical applications, *Mater. Sci. Eng. C.* 52 (2015) 22–30. <https://doi.org/10.1016/j.msec.2015.03.027>.
- [39] R.F. Landel, Mechanical properties of a polyurethane elastomer in the rubber-to-glass transition zone, *J. Colloid Sci.* 12 (1957) 308–320. [https://doi.org/10.1016/0095-8522\(57\)90016-8](https://doi.org/10.1016/0095-8522(57)90016-8).
- [40] J.H.Y. Chung, M.L.W. Knetsch, L.H. Koole, A. Simmons, L.A. Poole-Warren, Polyurethane Organosilicate Nanocomposites as Blood Compatible Coatings, *Coatings.* 2 (2012) 45–63. <https://doi.org/10.3390/coatings2010045>.
- [41] R. Iskakov, E.O. Batyrbekov, M.B. Leonova, B.A. Zhubanov, Preparation and release profiles of cyclophosphamide from segmented polyurethanes, *J. Appl. Polym. Sci.* 75 (2000) 35–43. [https://doi.org/10.1002/\(SICI\)1097-4628\(20000103\)75:1<35::AID-APP5>3.0.CO;2-2](https://doi.org/10.1002/(SICI)1097-4628(20000103)75:1<35::AID-APP5>3.0.CO;2-2).

- [42] H. Janik, M. Marzec, A review: Fabrication of porous polyurethane scaffolds, *Mater. Sci. Eng. C.* 48 (2015) 586–591. <https://doi.org/10.1016/j.msec.2014.12.037>.
- [43] ASTM Standard D882-18: Test Method for Tensile Properties of Thin Plastic Sheeting, (2018). <https://www.astm.org/Standards/D882>.
- [44] ASTM Standard D1708-96: Test Method for Tensile Properties of Plastics by Use of Microtensile Specimens, (2002). <https://www.astm.org/DATABASE.CART/HISTORICAL/D1708-96.htm>.
- [45] B. Shah, V.K. Kakumanu, A.K. Bansal, Analytical techniques for quantification of amorphous/crystalline phases in pharmaceutical solids, *J. Pharm. Sci.* 95 (2006) 1641–1665. <https://doi.org/10.1002/jps.20644>.
- [46] C. Wilhelm, J.-L. Gardette, Infrared analysis of the photochemical behaviour of segmented polyurethanes: aliphatic poly(ether-urethane)s, *Polymer*. 39 (1998) 5973–5980. [https://doi.org/10.1016/S0032-3861\(97\)10065-9](https://doi.org/10.1016/S0032-3861(97)10065-9).
- [47] C. Wilhelm, J.-L. Gardette, Infrared analysis of the photochemical behaviour of segmented polyurethanes: 1. Aliphatic poly(ester-urethane), *Polymer*. 38 (1997) 4019–4031. [https://doi.org/10.1016/S0032-3861\(96\)00984-6](https://doi.org/10.1016/S0032-3861(96)00984-6).
- [48] Q. Tang, K. Gao, Structure analysis of polyether-based thermoplastic polyurethane elastomers by FTIR, <sup>1</sup>H NMR and <sup>13</sup>C NMR, *Int. J. Polym. Anal. Charact.* 22 (2017) 569–574. <https://doi.org/10.1080/1023666X.2017.1312754>.
- [49] A. Srivastava, P. Arya, S. Goel, B. Kundu, P. Mishra, A. Fnu, Gelsolin Amyloidogenesis Is Effectively Modulated by Curcumin and Emetine Conjugated

PLGA Nanoparticles, PLOS ONE. 10 (2015) e0127011.

<https://doi.org/10.1371/journal.pone.0127011>.

- [50] D.S. Trifan, J.F. Terenzi, Extents of hydrogen bonding in polyamides and polyurethanes, *J. Polym. Sci.* 28 (1958) 443–445.  
<https://doi.org/10.1002/pol.1958.1202811727>.
- [51] K. Knutson, D.J. Lyman, The Effect of Polyether Segment Molecular Weight on the Bulk and Surface Morphologies of Copolyether-Urethane-Ureas, in: *Biomater. Interfacial Phenom. Appl.*, American Chemical Society, 1982: pp. 109–132.  
[https://www.researchgate.net/publication/288916180\\_The\\_Effect\\_of\\_Polyether\\_Segment\\_Molecular\\_Weight\\_on\\_the\\_Bulk\\_and\\_Surface\\_Morphologies\\_of\\_Copolyether-Urethane-Ureas](https://www.researchgate.net/publication/288916180_The_Effect_of_Polyether_Segment_Molecular_Weight_on_the_Bulk_and_Surface_Morphologies_of_Copolyether-Urethane-Ureas).
- [52] I. Rehman, C. Barnardo, R. Smith, Fourier transform infrared analysis of poly(ester-urethanes) at low temperature in-situ by using a newly constructed liquid nitrogen cooled sample stage, *J. Mater. Sci.* 32 (1997) 2617–2621.  
<https://doi.org/10.1023/A:1018610719598>.
- [53] P. Król, B. Król, Surface free energy of polyurethane coatings with improved hydrophobicity, *Colloid Polym. Sci.* 290 (2012) 879–893.  
<https://doi.org/10.1007/s00396-012-2598-x>.
- [54] J. Coates, Interpretation of Infrared Spectra, A Practical Approach, *Encycl. Anal. Chem.* (2006). <https://doi.org/10.1002/9780470027318.a5606>.

- [55] D. Rosu, L. Rosu, C.N. Cascaval, IR-change and yellowing of polyurethane as a result of UV irradiation, *Polym. Degrad. Stab.* 94 (2009) 591–596.  
<https://doi.org/10.1016/j.polymdegradstab.2009.01.013>.
- [56] A. Mishra, P. Maiti, Aromatic polyurethanes: the effect of hard segment and chain structure on their properties, *J. Polym. Eng.* 31 (2011) 253–259.  
<https://doi.org/10.1515/polyeng.2011.051>.
- [57] D.J. Martin, G.F. Meijs, G.M. Renwick, S.J. Mccarthy, P.A. Gunatillake, The effect of average soft segment length on morphology and properties of a series of polyurethane elastomers. I. Characterization of the series, *J. Appl. Polym. Sci.* 62 (1996) 1377–1386. [https://doi.org/10.1002/\(SICI\)1097-4628\(19961128\)62:9<1377::AID-APP7>3.0.CO;2-E](https://doi.org/10.1002/(SICI)1097-4628(19961128)62:9<1377::AID-APP7>3.0.CO;2-E).
- [58] K.-S. Chen, T. Leon Yu, Y.-S. Chen, T.-L. Lin, W.-J. Liu, Soft-and hard-segment phase segregation of polyester-based polyurethane, *J. Polym. Res.* 8 (2001) 99–109.  
<https://doi.org/10.1007/s10965-006-0139-3>.
- [59] T.R. Hesketh, J.W.C.V. Bogart, S.L. Cooper, Differential scanning calorimetry analysis of morphological changes in segmented elastomers, *Polym. Eng. Sci.* 20 (1980) 190–197. <https://doi.org/10.1002/pen.760200304>.
- [60] J.T. Koberstein, T.P. Russell, Simultaneous SAXS-DSC study of multiple endothermic behavior in polyether-based polyurethane block copolymers, *Macromolecules.* 19 (1986) 714–720. <https://doi.org/10.1021/ma00157a039>.



- [61] A. Lapprand, F. Méchin, J.-P. Pascault, Synthesis and properties of self-crosslinkable thermoplastic polyurethanes, *J. Appl. Polym. Sci.* 105 (2007) 99–113. <https://doi.org/10.1002/app.26086>.
- [62] Z.S. Petrović, L. Yang, A. Zlatanić, W. Zhang, I. Javni, Network structure and properties of polyurethanes from soybean oil, *J. Appl. Polym. Sci.* 105 (2007) 2717–2727. <https://doi.org/10.1002/app.26346>.
- [63] H. Fu, Y. Wang, X. Li, W. Chen, Synthesis of vegetable oil-based waterborne polyurethane/silver-halloysite antibacterial nanocomposites, *Compos. Sci. Technol.* 126 (2016) 86–93. <https://doi.org/10.1016/j.compscitech.2016.02.018>.
- [64] N.J. Clayden, C. Nijs, G. Eeckhaut, Study of the Polymer Morphology in Urethane Elastomers by Solid State 2H NMR and Small Angle X-ray Scattering, *Macromolecules*. 31 (1998) 7820–7828. <https://doi.org/10.1021/ma9709009>.
- [65] R. Androsch, J. Blackwell, S.N. Chvalun, G. Festel, C.D. Eisenbach, X-Ray investigation of the structure of polyurethane elastomers based on 1,5-naphthalene diisocyanate, *Acta Polym.* 48 (1997) 363–368. <https://doi.org/10.1002/actp.1997.010480903>.
- [66] K.M. Zia, I.A. Bhatti, M. Barikani, M. Zuber, M.A. Sheikh, XRD studies of chitin-based polyurethane elastomers, *Int. J. Biol. Macromol.* 43 (2008) 136–141. <https://doi.org/10.1016/j.ijbiomac.2008.04.009>.
- [67] V.S.C. Chang, J.P. Kennedy, Gas permeability, water absorption, hydrolytic stability and air-oven aging of polyisobutylene-based polyurethane networks, *Polym. Bull.* 8 (1982) 69–74. <https://doi.org/10.1007/BF00263010>.

- [68] K.M. Zia, M. Barikani, M. Zuber, I.A. Bhatti, H.N. Bhatti, Morphological Studies of Polyurethane Elastomers Extended with  $\alpha,\omega$  Alkane Diols, Iran. Polym. J. 17 (2008) 61–72.
- [69] G. Gultekin, C. Atalay-Oral, S. Erkal, F. Sahin, D. Karastova, S.B. Tantekin-Ersolmaz, F.S. Guner, Fatty acid-based polyurethane films for wound dressing applications, J. Mater. Sci. Mater. Med. 20 (2009) 421–431.  
<https://doi.org/10.1007/s10856-008-3572-5>.
- [70] A. Boubakri, K. Elleuch, N. Guermazi, H.F. Ayedi, Investigations on hygrothermal aging of thermoplastic polyurethane material, Mater. Des. 30 (2009) 3958–3965.  
<https://doi.org/10.1016/j.matdes.2009.05.038>.
- [71] Z. Chen, I.-C. Peng, X. Cui, Y.-S. Li, S. Chien, J.Y.-J. Shyy, Shear stress, SIRT1, and vascular homeostasis, Proc. Natl. Acad. Sci. 107 (2010) 10268–10273.  
<https://doi.org/10.1073/pnas.1003833107>.
- [72] Guo Deliang, Chien Shu, Shyy John Y.-J., Regulation of Endothelial Cell Cycle by Laminar Versus Oscillatory Flow, Circ. Res. 100 (2007) 564–571.  
<https://doi.org/10.1161/01.RES.0000259561.23876.c5>.
- [73] P. Davies, How Do Vascular Endothelial Cells Respond to Flow?, Physiology. 4 (1989) 22–25. <https://doi.org/10.1152/physiologyonline.1989.4.1.22>.
- [74] H.J. Qi, M.C. Boyce, Stress–strain behavior of thermoplastic polyurethanes, Mech. Mater. 37 (2005) 817–839. <https://doi.org/10.1016/j.mechmat.2004.08.001>.

- [75] S.F. Chou, R.A. Overfelt, Tensile deformation and failure of North American porcupine quills, *Mater. Sci. Eng. C*. 31 (2011) 1729–1736.  
<https://doi.org/10.1016/j.msec.2011.08.002>.
- [76] P. Jutrzenka Trzebiatowska, A. Santamaria Echart, T. Calvo Correias, A. Eceiza, J. Datta, The changes of crosslink density of polyurethanes synthesised with using recycled component. Chemical structure and mechanical properties investigations, *Prog. Org. Coat.* 115 (2018) 41–48. <https://doi.org/10.1016/j.porgcoat.2017.11.008>.
- [77] Y. Yanagihara, N. Osaka, S. Iimori, S. Murayama, H. Saito, Relationship between modulus and structure of annealed thermoplastic polyurethane, *Mater. Today Commun.* 2 (2015) e9–e15. <https://doi.org/10.1016/j.mtcomm.2014.10.001>.
- [78] A. Stribeck, E. Pösel, B. Eling, F. Jokari-Sheshdeh, A. Hoell, Thermoplastic polyurethanes with varying hard-segment components. Mechanical performance and a filler-crosslink conversion of hard domains as monitored by SAXS, *Eur. Polym. J.* 94 (2017) 340–353. <https://doi.org/10.1016/j.eurpolymj.2017.07.020>.
- [79] K. Kojio, M. Furukawa, Y. Nonaka, S. Nakamura, Control of Mechanical Properties of Thermoplastic Polyurethane Elastomers by Restriction of Crystallization of Soft Segment, *Materials*. 3 (2010) 5097–5110. <https://doi.org/10.3390/ma3125097>.
- [80] P. Ross, G. Sevilla, J. Quagliano, Effect of chain extender on the mechanical and thermal resistance properties of polyurethane liners for composite propellants, *Polyurethanes*. 1 (2016). <https://doi.org/10.1515/polyur-2017-0001>.
- [81] Moon, Suk-Young, Park, Young-Deok, Kim, Cheul Ju, Won, Chan-Hee, Lee, Youn Sik, Effect of Chain Extenders on Polyurethanes Containing Both Poly(butylene

succinate) and Poly(ethylene glycol) as Soft Segments, Bull. Korean Chem. Soc. 24 (2003) 1361–1364. <https://doi.org/10.5012/BKCS.2003.24.9.1361>.